EBioMedicine 48 (2019) 143–160

Contents lists available at ScienceDirect

EBioMedicine

journal homepage: www.elsevier.com/locate/ebiom

EBioMedicine
Published by THE LANCET

Variants in oxidative stress-related genes affect the chemosensitivity through Nrf2-mediated signaling pathway in biliary tract cancer

Ming Zhan[a,1], Hui Wang[a,1], Sun-Wang Xu[a,1], Lin-Hua Yang[a,1], Wei Chen[a], Shuang-Xia Zhao[b], Hui Shen[a], Qiang Liu[c], Rui-Meng Yang[b,*], Jian Wang[a,*]

[a] Department of Biliary-Pancreatic Surgery, Renji Hospital, School of Medicine, Shanghai Jiao Tong University, Shanghai 200127, China
[b] The Core Laboratory in Medical Center of Clinical Research, Department of Endocrinology, Shanghai Ninth People's Hospital, State Key Laboratory of Medical Genomics, Shanghai Jiao Tong University (SJTU) School of Medicine, Shanghai 200011, China
[c] Department of Pathology, Renji Hospital, School of Medicine, Shanghai Jiao Tong University, Shanghai 200127, China

ARTICLE INFO

Article history:
Received 14 June 2019
Revised 15 August 2019
Accepted 18 August 2019
Available online 4 October 2019

Keywords:
Biliary tract cancer
Single nucleotide polymorphism
Oxidative stress
Nrf2
Chemosensitivity

ABSTRACT

Background: Oxidative stress and their effectors play critical roles in carcinogenesis and chemoresistance. However, the role of oxidative stress-related genes variants in biliary tract cancer (BTC) chemoresistance remains unknown. In this work, we aim to investigate oxidative stress-dependent molecular mechanisms underlying chemoresistance, and find potential biomarkers to predict chemotherapy response for BTC.

Methods: Sixty-six SNPs in 21 oxidative stress-related genes were genotyped and analyzed in 367 BTC patients. Immunoblot, immunohistochemical, immunofluorescent, quantitative PCR, chromatin immunoprecipitation analysis and study of animal xenograft models were performed to discover oxidative stress-related susceptibility genes underlying chemoresistance mechanism of BTC.

Findings: We found that 3 functional polymorphisms (*CAT*_rs769217, *GPX4*_rs4807542, and *GSR*_rs3779647), which were shown to affect their respective gene expression levels, modified the effect of chemotherapy on overall survival (OS). We then demonstrated that knockdown of *GPX4*, *CAT*, or *GSR* induced chemoresistance through elevation of ROS level and activation of Nrf2-ABCG2 pathway in BTC cell lines. Moreover, the association between Nrf2 expression and BTC prognosis is only found in patients who received chemotherapy. Knockdown of Nrf2 enhanced chemosensitivity or even eliminated postoperative recurrence in BTC xenograft mouse models. Importantly, upon chemotherapy treatment patients harboring high oxidative stress-related score received higher survival benefit from adjuvant chemotherapy compared with patients with low oxidative stress-related score.

Interpretation: The result of our study suggests, for the first time, that the oxidative stress-related score calculated by combining variations in *CAT*, *GPX4*, and *GSR* or Nrf2 expression could be used for predicting the chemosensitivity of BTC patients.

Fund: This work was supported by the National Science Foundation of China, Foundation of Shanghai Shen Kang Hospital Development Center, and Shanghai Outstanding Academic Leaders Plan.

Research in context

Evidence before this study

A disrupted cellular redox state is a common feature of most tumors including biliary tract cancer (BTC). Reactive oxygen species (ROS) production induced oxidative stress has been reported to affect BTC initiation, progression and chemotherapeutic effects. In previous studies, we confirmed that ROS played an important role in regulating the

* Corresponding authors.
E-mail addresses: yangrm1990@163.com (R.-M. Yang), dr_wangjian@126.com (J. Wang).
[1] These authors contributed equally to the work.

https://doi.org/10.1016/j.ebiom.2019.08.037

chemosensitivity of BTC cells. However, the mechanism leading to the chemoresistance mediated by ROS and the underlying functional remain unclear.

Added value of this study

The genetic variations in somatic tumor cells have been shown correlated with patients' chemotherapy response. In this study, three single nucleotide polymorphisms (SNPs) located in *GPX4*, *CAT* and *GSR* were found to specifically influence the prognosis in BTC patients treated with adjuvant chemotherapy. In human BTC specimens, correlations between the *GPX4*, *CAT* and *GSR* variants with their respective expression levels were also found. In addition, silencing of *GPX4*, *CAT* and *GSR*, which mimic the effect of variants on expression, promoted cancer cell proliferation and chemoresistance through elevating ROS levels and subsequently activating Nrf2 related pathways.

Implications of all the available evidence

Our study provides new insights into understanding the impact of polymorphisms in oxidative stress-related genes on chemotherapy sensitivity of BTC patients. Our findings also imply that oxidative stress-related factors may be considered for future individualized chemotherapy of patients with malignant tumors.

1. Introduction

Biliary tract cancer (BTC), encompassing intrahepatic cholangiocarcinoma (CC), perihilar CC, distal CC, and gallbladder cancer (GBC), is a common malignant neoplasm of the digestive tract with poor prognosis [1]. Although biological behavior, molecular basis and pathogenesis of different BTC subgroups may be different, high chemoresistance rate is one of the common themes shared by all BTC subgroups, and is associated with lower 5-year survival rate (10% for CCs and <5% for GBC) [2,3]. Therefore, understanding the underlying mechanisms of BTC chemoresistance and tumor relapse is critical for treating and developing novel therapeutics for BTC.

In recent years, genome-wide association studies (GWAS) have identified multiple genetic loci associated with complicated diseases like cancer [4]. Increasing evidences suggest that many of the single nucleotide polymorphisms (SNPs), though may exhibit modest effect when solo, however, when present in combination, may have a larger impact in particular circumstances, such as response to chemotherapeutic treatment [5]. A disrupted cellular redox state is a common feature of most tumors including GBC and CCs [6,7]. Compelling evidence suggest that reactive oxygen species (ROS) production induced oxidative stress can act as "messenger" which is implicated in tumor initiation, progression and chemoresistance [8]. While ROS-mediated mechanisms of action represent a major cancer-targeting strategy, emerging data indicate that chronic and abnormally high ROS levels may instigate or accentuate cancer phenotypes, including chemoresistance [9]. Nuclear factor E2-related factor 2 (Nrf2) and other antioxidant genes, such as glutathione peroxidases (GPXs), glutathione reductase (GSR), catalase (CAT), are involved in cellular defense and survival against oxidative stress. A number of studies have found that oxidative stress is closely related with the occurrence of many types of biliary tract diseases including biliary system inflammation, stone, and cancer [6,10]. Whether "intrinsic" genetic polymorphisms of oxidative stress-related genes influences chemotherapeutic response of BTC and how related functional genomic variants exert their function still have not been investigated.

In this study, variants in 3 antioxidant-related genes (*GPX4*_rs4807542 and *GSR*_rs3779746 in GBC; *CAT*_rs769217 and *GSR*_rs3779746 in CC) were found to specifically influence the prognosis in BTC patients treated with adjuvant chemotherapy. Correlations between the *GPX4*, *CAT* and *GSR* variants and their expression levels were found in BTC specimens. Further in vitro mechanisms study we found that reduced *GPX4*, *CAT* and *GSR* expression could modify the chemosensitivity through ROS dependent Nrf2 pathway activation. In conclusion, our results provide evidence for the influential role of oxidative stress-related genes variants in modifying the effects of adjuvant chemotherapy in BTC.

2. Materials and methods

2.1. Patients, samples and follow-up data

We retrospectively recruited a set of patients with no prior history of cancer and newly diagnosed with BTC, including distal CC, perihilar CC, intrahepatic CC, and GBC, in Renji hospital from January 2002 to December 2013. All participants underwent computed tomography scans. Pathology slides obtained for each subject were reviewed by two pathologists from our hospital. After reviewing of imaging data, medical records, surgical reports, and pathology slides by a panel of clinicians, and pathologists, a total of 367 unrelated subjects that were confirmed with the diagnosis of BTCs were enrolled for the association analysis in this study. At enrollment, data on epidemiologic factors were collected by in-person or telephone interview, and detailed clinical data, such as preoperative laboratory, operative details, and pathologic were collected from electronic or paper medical records and retrospective interviews. The main postoperative chemotherapy drug include 5-Fu, doxorubicin, cisplatin, oxaliplatin, and gemcitabine. Approximately 85% and 80% of the patients that were treated with chemotherapy received gemcitabine and platinum-based regimens, respectively. The strategy of systemic treatments was updated according to the National Comprehensive Cancer Network guidelines [11]. Patient's follow-up data were completed by June 2014, with a minimum follow-up period of 6 months or until death. Finally, we collected clinical data of each patient, including gender, age at primary diagnosis of BTC, smoking history, drinking history, gallstone status, diabetes status, CA19–9 level, tumor size, tumor metastasis, Ki-67 staining, P53 staining, tumor differentiation, operation mode, postoperative adjuvant chemotherapy, and overall survival (OS). The basic demographical and clinical features of the 367 BTC patients are presented in Table 1.

Tumor tissue samples (178 GBC and 189 CC) were collected from patients who underwent surgical resection of the biliary tract. Each of the tumor tissue was paraffin embedded, and was used to isolate genomic DNA and immunohistochemical (IHC) staining. Of the 367 subjects, only 88 fresh tumor tissues (36 GBC and 52 CC) were collected and stored in liquid nitrogen for RNA extraction and expression analysis, and their peripheral blood were also obtained and used for total DNA isolation.

This study was granted approval by the Ethical Committee of the Renji hospital, Shanghai Jiao Tong University School of Medicine. All of the subjects in this study provided written informed consent according to the protocols approved by the Ethics Committees, and their data were analyzed anonymously.

2.2. SNP selection

The SNPs included in this study were selected on the basis of literature evidence suggesting possible functional consequences or previous association studies showing a link between oxidative stress and cancer. Finally, a total of 66 polymorphisms were analyzed from candidate 21 genes, which showing in Supplementary

Table 1
Selected clinical data of BTC patients.

Characteristic	BTC	Gallbladder cancer	Cholangiocarcinoma	*P* value
	(*n* = 367)	(*n* = 178)	(*n* = 189)	
Follow-up time, mo				
Median (ranges)	10.2 (0.2–101.9)	9.1 (0.2–93.2)	12.1 (0.2–101.9)	[a]0.121
Gender				
Female, n (%)	202 (55.0)	118 (66.3)	84 (44.4)	<0.001
Male, n (%)	165 (45.0)	60 (33.7)	105 (55.6)	
Age, y				
Mean ± SD	64.4 ± 11.8	66.1 ± 11.5	62.8 ± 11.8	0.008
≥ 60, n (%)	243 (66.2)	132 (74.2)	111 (58.7)	0.002
< 60, n (%)	124 (33.8)	46 (25.8)	78 (41.3)	
Median (ranges)	64 (16–88)	67 (33–86)	62 (16–88)	
Ever smoke				
Yes, n (%)	117 (31.9)	43 (24.2)	74 (39.2)	0.002
No, n (%)	250 (68.1)	135 (75.8)	115 (60.8)	
Ever drink alcohol				
Yes, n (%)	96 (26.2)	33 (18.5)	63 (33.3)	0.001
No, n (%)	271 (73.8)	145 (81.5)	126 (66.7)	
Gallstone status				
Yes, n (%)	274 (74.7)	144 (80.9)	130 (68.8)	0.008
No, n (%)	93 (25.3)	34 (19.1)	59 (31.2)	
Diabetes				
Yes, n (%)	43 (11.7)	21 (11.8)	22 (11.6)	0.963
No, n (%)	324 (88.3)	157 (88.2)	167 (88.4)	
CA19–9, U/ml				
≥ 37, n (%)	268 (73.0)	109 (61.2)	159 (84.1)	<0.001
< 37, n (%)	99 (27.0)	69 (38.8)	30 (15.9)	
Tumor size, cm				
≥ 5, n (%)	111 (30.2)	58 (32.6)	53 (28.0)	0.344
< 5, n (%)	256 (69.8)	120 (67.4)	136 (72.0)	
Tumor metastasis				
Yes, n (%)	223 (60.8)	107 (60.1)	116 (61.4)	0.804
No, n (%)	144 (39.2)	71 (39.9)	73 (38.6)	
Ki-67				
Negative, n (%)	62 (16.9)	17 (9.6)	45 (23.8)	<0.001
Positive, n (%)	305 (83.1)	161 (90.4)	144 (76.2)	
P53				
Negative, n (%)	176 (48.0)	85 (47.8)	91 (48.1)	0.940
Positive, n (%)	191 (52.0)	93 (52.2)	98 (51.9)	
Tumor differentiation				
Well, n (%)	45 (12.3)	26 (14.6)	19 (10.1)	0.184
Moderate, poor or undifferentiated, n (%)	322 (87.7)	152 (85.4)	170 (89.9)	
Radical surgery				
Yes, n (%)	268 (73.0)	105 (59.0)	163 (86.2)	<0.001
No, n (%)	99 (27.0)	73 (41.0)	26 (13.8)	
Chemotherapy				
Yes, n (%)	159 (43.3)	82 (46.1)	77 (40.7)	0.303
No, n (%)	208 (56.7)	96 (53.9)	112 (59.3)	

BTC, biliary tract cance; GBC, gallbladder cancer; CC, cholangiocarcinoma.
[a] Multivariate Cox proportional hazards regression analyses were adjusted for gender, age (≥60 y or <60 y), ever smoke (yes or no), ever drink alcohol (yes or no), gallstone status (yes or no), diabetes (yes or no), CA19–9 (≥37 U/ml or <37 U/ml), tumor size (≥5 cm or <5 cm), tumor metastasis (yes or no), Ki-67 (positive or negative staining by IHC), P53 (positive or negative staining by IHC), tumor differentiation (well or moderate, poor or undifferentiated), radical surgery (positive or negative), and chemotherapy (yes or no).

Table 1. The list of genes comprised *CAT*, *CYBA*, *GCLM*, *GPX1*, *GPX2*, *GPX3*, *GPX4*, *GSR*, *GSTP1*, *HMOX1*, *KEAP1*, *MPO*, *NFE2L2*, *NOS1*, *NOS2*, *NOS3*, *NQO1*, *NQO2*, *SOD1*, *SOD2*, and *SOD3*. We chose the SNPs that are not only within gene bodies, but also those in the 5′ and 3′ flanking regions up to 5 kb. All polymorphisms had a minor allele frequency greater than or equal to 5% in a population of Asian descendents (in the 1000 Genomes ASN samples). Information about the selected SNPs were collected from two public databases: NCBI dbSNP database (http://www.ncbi.nlm.nih.gov/snp/) and HapMap (http://www.hapmap.org).

2.3. DNA preparation and genotyping

Genomic DNA was isolated from formalin-fixed paraffin-embedded (FFPE) tissue samples with QIAamp DNA FFPE Tissue Kit (Qiagen, Hilden, Germany) according to the manufacturer's instructions. Genomic DNA was also extracted from the blood samples using QuickGene DNA whole blood kit S at FUJIFILM QuickGene-610 L system platform (FUJIFILM, Tokyo, Japan) as previously described [12,13]. The concentrations of DNA were quantified using Nanodrop 8000 (Thermo Fisher Scientific Inc., Waltham, MA). The concentrations of the DNA samples used in this study were ≥50 ng/μL and the A260/A280 ratio of the DNA samples was between 1.6 and 1.8.

For SNP genotyping, 50 ng/μl of DNA was used for all samples, and one negative control (DNase-free and RNase-free water) was included in a random well on the 96 wells plate. Fourty-eight SNPs were genotyped using the TaqMan assay on Applied Biosystems ViiATM 7 Real-Time PCR System (Applied Biosystems, Foster City, CA, USA) according to the manufacturer's instructions. Post-polymerase chain reaction allelic discrimination was performed by measuring the allele-specific fluorescence. The average call rate from TaqMan assay was >95%. Samples without outcome in TaqMan assay and

the other 18 SNPs were genotyped by PCR-sequencing. In addition, eighty-eight samples were selected for repeated genotyping using tissue and blood DNA, and the results were 100% concordant. All the genotyping experiments were conducted by technicians who were blinded to the sample status. In this study, genotype frequencies of each SNP were consistent with Hardy-Weinberg equilibrium, checked by standard χ^2 test using a web-based software (http://ihg.gsf.de/cgi-bin/hw/hwa1.pl).

2.4. OS association analysis and receiver operating characteristics curve

OS was calculated from the date of diagnosis to the date of last follow-up or death. The association of the genotypes of 66 SNPs with OS was analyzed by the dominant model (major homozygous vs. heterozygous & minor homozygous). Kaplan-Meier method with the log-rank test (univariate analysis) and Cox proportional hazards regression model (multivariate analysis) were used to analysis the association between OS and genotype. Patients with study end date were considered to be censored. HR for disease progression and 95% CIs were calculated by the Cox risk proportion model. Interactions between the 6 selected variants (in the dominant model) and chemotherapy in GBC and CC were investigated by multivariate Cox regression analysis along with adjustment for the significant independent factors of OS.

To construct the prediction model for OS, we developed a combined "oxidative stress-related score" by assigning "0" to risk factor and "1" to protective factor of the susceptible variants (GBC: rs4807542, rs8190996, rs3779647, and rs2978663; CC: rs769217, rs3779647, rs2978663, and rs2978662) and Nrf2 expression. We also developed a combined "clinical score" by assigning a set of clinical features associated with prognosis, such as tumor size, tumor metastasis, P53 staining, tumor differentiation, and operation mode. The "total score" is the sum of oxidative stress-related score and clinical score. Thus, each patient had oxidative stress-related score ranging from 0 to 5, clinical score ranging from 0 to 5, and total score ranging from 0 to 10. In addition, we divided patients into 2 groups (score 0–2, and score 3–5) according to oxidative stress-related score for the OS association analysis.

To further evaluate the accuracy of the prediction model for OS, receiver operating characteristics (ROC) [14] curves were generated, and the area under the curve (AUC) with its 95% confidence intervals (CIs) and Youden-index for the overall accuracy of screening test, was also calculated. The ROC curve shows the relation between sensitivity and false-positive rate (1-specificity) of a given test across all possible threshold values that define the positivity of a disease or condition. In ROC analysis, the independent variable was survival outcome (GBC: OS >12 months or not; CC: OS >16 months or not), and the classification variable is probability of disease progression, which was evaluated by "score" mentioned above. Two-tailed hypothesis tests were used for comparison between AUC.

All clinical data analyses were performed using the IBM SPSS Statistics analysis software, version 19.0 (IBM, NewYork, USA), and were based on two-tailed hypothesis tests with a significance level of $P < .05$.

2.5. Cell culture

The human GBC cell line GBC-SD was purchased from the Shanghai Institutes for Biological Sciences (Shanghai, China). The CC cell line QBC-939 was obtained from Prof. Shuguang Wang (The Third Military Medical University, China). Human embryonic kidney 293 cells (HEK293FT) were purchased from Invitrogen (Gaithersburg, MD, USA). Liquid nitrogen stocks were made upon receipt and maintained until the start of each study. Cells were used for no >3 months after being thawed. GBC-SD and HEK293FT were cultured in DMEM medium, and QBC-939 cells was cultured in RPMI-1640 medium, with all media containing 10% FBS, 100 units/ml penicillin and 100 mg/ml streptomycin (Gibco, Grand Island, NY). Cells were incubated at 37 °C in a humidified incubator under 5% CO_2 and tested negative for mycoplasma infection by LookOut® mycoplasma qPCR detection kit (Sigma, St. Louis, MO, USA).

2.6. Gene silencing and over-expression in GBC-SD and QBC-939

For temporary gene silencing, all siRNA compounds were chemically synthesized and stabilized by 2O'-Me modifications. The following Stable™ siRNA oligo (Genepharma, Shanghai, China) were used: nontargeting scrambled siRNA, human *GPX4* siRNA, human *CAT* siRNA, human *GSR* siRNA, and human *ABCG2* siRNA. For siRNA experiments, GBC-SD or QBC-939 cells were transfected with 100 pmol siRNA using Lipofectamine 2000 (Invitrogen, San Diego, CA) in 6-well plates following the manufacture's protocols. Transfection media was removed after 12 h. Transfected cells were cultured for 48 h before experiments.

For stable gene silencing, lentiviral vectors (pLKO.1-Puro, obtained from Addgene; Cambridge, MA, USA) were constructed to by introducing stem loop sequences of short hairpin RNA (shRNA) specifically targeting the human *NFE2L2*, or scrambled control sequence. Recombinant lentiviruses were produced by transient transfection of HEK293FT cells with lentiviral shRNA vector, along with package vectors, using Lipofectamine 2000. Then GBC-SD or QBC-939 cells were infected with lentiviruses in the presence of 6 μg/ml Polybrene (Sigma, St. Louis, MO, USA). At 24 h postinfection, cells were grown in the medium containing 2.0 μg/ml of puromycin (Invitrogen, San Diego, CA) for antibiotic selection. Once all the negative control cells were killed, stable cell lines were established and continuously needed to grown in the media containing the same concentration of puromycin.

Human *GPX4*, *CAT*, *GSR*, *ABCG2*, and *NFE2L2* expression construct was generated by insertion of their coding region at *Eco*RI-*Bgl*II sites in 3xFLAG-pCMV vector (Sigma, St. Louis, MO, USA) containing a neomycin-resistant gene. Then GBC-SD or QBC-939 cells were transfected with flag-tagged expression vector or empty vector as a control. The stable transfectants were screened for neomycin resistance by culturing in medium supplemented with G418 (750 μg/ml).

2.7. Cell cytotoxicity, proliferation, and apoptosis assays

The in vitro drug sensitivity to cisplatin and doxorubicin was assessed with 3-(4,5- dimethylthiazol-2-yl)-5-(3-Carboxymethoxyphenyl)-2-(sulfophenyl)-2H-tetrazolium (MTS) by using Cell Titer 96® AQueous One Solution Cell Proliferation Assay (Promega, Madison, WI, USA). GBC-SD or QBC-939 cells were plated at a density of 5×10^3 cells/well in 96-well plates, and were allowed to recover overnight and then exposed to various concentrations of doxorubicin for 48 h. After adding 20 μl of Cell Titer 96® Aqueous One Solution Reagent into each well (96-well plate) that contains the sample in 100 μl of culture medium, the plates were incubated at 37 °C in a humidified, 5% CO_2 atmosphere for 2 h, and absorbance at 490 nm was measured using a Synergy 2 (Biotek, Winooski, VT, USA) plate reader. Measurements were expressed as percentage change from untreated control of appropriate cells. Each combination of cell line and drug concentration was repeated eight times. IC50 was calculated as the concentration that reduced viability by 50%.

Cellular proliferation assay was also carried out using the Cell Titer 96® AQueous One Solution Cell Proliferation Assay kit. Briefly,

GBC-SD or QBC-939 cells (1000 cells/well) were plated in 96-well plates and the growth rate was measured in the following 7 days.

For apoptosis analysis, Annexin V/propidium iodide (PI) staining also was performed by using flow cytometry according to the manufacturer's guidelines (BD Biosciences, Bedford, MA, USA). GBC-SD or QBC-939 cells were seeded in 6-well plates, and were grown to approximately 60% confluence, followed by treating with cisplatin for 48 h. Then the floating and attached cells were harvested and incubated with Annexin-V and PI prior to FACS apoptosis analysis. For each sample, 10^4 cells were examined. The percentage of apoptotic and necrotic cells was determined by statistical analysis of the various dot plots FlowJo software (Tree Star, Ashland, OR, USA).

2.8. mRNA expression analysis

In the mRNA expression analyses of clinical specimens, 36 GBC tissues and 52 tissues samples were surgically collected from patients. Total RNA in tissue or cell was isolated using Trizol reagent (Invitrogen, San Diego, CA) according to the manufacturer's instructions and then treated with DNase I at room temperature for 10 min to degrade possible contaminating genomic DNA. cDNAs were made from 1 μg RNA templates using reverse transcriptase (Takara, Shiga, Japan) and oligo(dT) primer. qPCR for a series of genes was performed in triplicate using SYBR Green PCR Master Mix and run with Applied Biosystems ViiA™ 7 Real-Time PCR System (Applied Biosystems, Foster City, CA, USA). PCR conditions included an initial denaturation step of 5 min at 95 °C, followed by 40 cycles of PCR consisting of 5 s at 95 °C, 60 s at 60 °C. Data were analyzed by $2^{-\Delta\Delta CT}$ method [15] and were presented relative to the expression of the GAPDH housekeeping gene. The primer sequences used for qPCR are shown in the Supplementary Table 7.

2.9. Immunoblot analysis

For immunoblots, protein from GBC-SD and QBC-939 cells was extracted using RIPA buffer supplemented with a proteinase inhibitor cocktail (Sigma, St. Louis, MO, USA). Protein concentrations were estimated using the BCA method. Equal quantities of protein lysates were separated by SDS-PAGE and transferred onto polyvinylidene fluoride (PVDF) membranes (Millipore, Chicago, IL, USA). The membranes were blocked with Tris-bufferred saline with 0.05% Tween 20 and 5% skimmed milk, and then the following antibodies were applied overnight at 4 °C: anti-GPX4, anti-GSR, and anti-Nrf2 (Santa Cruz Biotechnology, Santa Cruz, CA, USA), anti-CAT and anti-NQO1 (Abcam, Cambridge, MA, USA), anti-ABCG2 and anti-β-actin (Sigma, St. Louis, MO, USA). After extensive washing, blots were then incubated with anti–mouse or anti-rabbit HRP-conjugated secondary antibody (Sigma, St. Louis, MO, USA) and visualized by chemiluminescence.

2.10. Immunohistochemistry analysis

All specimens fixed in 10% buffered formalin were embedded in paraffin blocks. Tumor sections (4 μm thick) were processed using a standard immunostaining protocol, and stained with the following antibodies: GPX4 (1:100, Santa Cruz Biotechnology, Santa Cruz, CA, USA), CAT (1:100, Santa Cruz Biotechnology, Santa Cruz, CA, USA), GSR (1:50, Santa Cruz Biotechnology, Santa Cruz, CA, USA), and Nrf2 (1:200, Santa Cruz Biotechnology, Santa Cruz, CA, USA) in formalin-fixed paraffin-embedded (FFPE) GBC and CC specimens, and Ki-67 (1:50 Abcam, Cambridge, MA, USA), Nrf2 (1:100, Santa Cruz Biotechnology, Santa Cruz, CA, USA), and ABCG2 (1:50, Santa Cruz Biotechnology, Santa Cruz, CA, USA) in FFPE tumor xenograft from nude mouse. After routine deparaffinization, hydration by ethanol gradient and blockage of endogenous peroxidase in hydrogen peroxide, sections were pretreated by microwave for 20 min in 10 mmol/L sodium citrate buffer (pH 6.0) for antigen retrieval. Then sections were blocked using the blocking agent (5% BSA), prior to overnight incubation at 4 °C with primary antibody mentioned above. Next day slides were washed thrice with PBS and incubated with secondary antibody (1:200, Promega, Madison, WI, USA) for 2 h at room temperature. After thrice PBS washing slides were incubated with streptavidin biotin-peroxidase complex (SABC) at room temperature for 30 min. Positive staining cells were visualized by 3,3-diaminobenzidine tetrahydrochloride (DAB) and counterstained with haematoxylin. Negative controls were incubated with PBS. The stained sections were photographed and converted to a digital image using light microscopy equipped with camera (Olympus CX31, Tokyo, Japan). The scoring system used was a semi-quantitative method that is based upon the staining intensity (I) and the proportion of tumor cells stained quantity (q) to obtain a final score (Q) defined as the product of I × q. The scoring system for I was: 0 = negative, 1 = low, 2 = moderate, 3 = intense immunostaining. The scoring system for q was: 0 = negative, 1 = 1–9% positive, 2 = 10–39% positive, 3 = 40–69% positive, 4 = 70–100% positive cells. Scoring was performed by two independent pathologists. In the analyses, Nrf2 expression was divided in 2 groups: low expression ($Q \leq 3$) and high expression ($Q > 3$).

2.11. Immunofluorescence assays

Cells were seeded in 12-well plates containing autoclaved glass coverslips and cultured in DMEM or RPMI-1640 medium containing 10% FBS. After thrice PBS washing, cells were covered with ice-cold 100% methanol for 10 min at −20 °C, and rinsed in PBS for 5 min. Then cells were blocked in Blocking Buffer (1 × PBS/5% normal serum/0.3% Triton™ X-100) for 60 min at room temperature, prior to incubating with primary antibody (Nrf2, 1:100; ABCG2, 1:50; Santa Cruz Biotechnology, Santa Cruz, CA, USA) overnight at 4 °C. Finally, cells were rinsed thrice in PBS, and incubated in fluorochrome-conjugated secondary antibody diluted in Antibody Dilution Buffer (1 × PBS/1% BSA/0.3% Triton X-100) for 2 h at room temperature in dark. Nuclei were counterstained with 4,6- diamidino-2-phenylindole (DAPI). Confocal laserscanning microscopy was performed using a Leica TCS SP5 confocal microscope (Leica, Mannheim, Germany).

2.12. Cellular ROS measurement

Cellular ROS was measured according to published protocols [16]. Briefly, GBC-SD and QBC-939 cells were washed with PBS and incubated with 5 μM CM-H2DCFDA (2′,7′-dichlorodihydrofluorescein diacetate; Invitogen) for 30 min at 37 °C. After washing thrice with PBS, cells were trypsinized and harvested, and then were kept on ice for an immediate detection by flow cytometer FACS Calibur (BD Biosciences, Bedford, MA, USA). DCF-DA fluorescence was analyzed by FlowJo software (Tree Star, Ashland, OR, USA). In case of sorted GBC-SD and QBC-939 cells, data were shown in the form of histogram overlays using the %Max option, which scaled each population curve to mode = 100% on the y axis, and log10 FL-1 (DCF-DA) fluorescence intensity on the x axis. Cells not incubated with the dye was used as ROS-negative control.

2.13. Determination of doxorubicin uptake

Flow cytometric analysis of doxorubicin uptake was carried out as previously described [6]. GBC-SD and QBC-939 cells were incubated with doxorubicin (1 mg/mL) for 1 h at 37 °C with shaking every 15 min avoiding light exposure. After rinsed twice with ice-cold PBS, cells were harvested using trypsin-EDTA and kept on ice. Doxorubicin uptake in cells was evaluated by recording of doxorubicin fluorescence (excitation at 488 nm; emission at 595 nm) in

flow cytometer FACS Calibur (BD Biosciences, Bedford, MA, USA). Cells without any drugs were used to assess the background fluorescence. A minimum of 10,000 events were collected for each sample. The fluorescence data were analyzed by FlowJo software (Tree Star, Ashland, OR, USA). The fluorescence intensity was expressed as GeoMean on the x axis, and the data of sorted cells were shown in the form of histogram overlays using the %Max option, which scaled each population curve to mode = 100% on the y axis. The net uptake of doxorubicin was measured using the fluorescence signal intensity of the treated cells subtracted with that of the cells without exposure to any drugs.

2.14. Terminal deoxynucleotidyl transferase dUTP nick end labeling (TUNEL) assays

Cell apoptosis from tumor xenograft was detected on sections by using In Situ Cell Death Detection Kit, POD (Roche Applied Science, Basel, Switzerland) according to manufacturer's instruction. Briefly, FFPE tumor xenograft from nude mouse were sectioned at 4 μm, and then deparaffinized by xylene and subsequently rehydrated by ethanol gradient. After thrice PBS washing, the sections were pretreated with proteinase K (20 μg/ml in 10 mM Tris/HCl) for 30 min, and blocked with 3% hydrogen peroxide in methanol for 10 min to eliminate endogenous POD. The sections were rinsed with PBS for 5 min twice, then incubated in dark with TUNEL reaction mixture for 60 min and Converter-POD solution for 30 mim at 37 °C. At last, positive staining cells were visualized by DAB and counterstained with haematoxylin. The DNA strand breaks during apoptosis were analyzed under a light microscope (Olympus CX31, Tokyo, Japan).

2.15. Dual-luciferase reporter assays

The Nrf2 antioxidant response element (ARE) or ABCG2 promoter fragment were inserted into the pGL3-promoter vector to generate the ARE-promoter plasmid as described previously [17]. In brief, *ABCG2* promoter region (−496 bp to +198 bp) was PCR amplified from human genomic DNA using high-fidelity Taq polymerase (Applied Biosystems, Foster City, CA). The ARE fragment was constructed by annealing of two DNA oligos. *ABCG2* promoter PCR product was cloned into the *Kpn*I and *Xho*I restriction sites, and the ARE was cloned into the *Hin*dIII and XhoI restriction sites of the pGL3 basic vector (Promega, Madison, WI, USA). Mutant ARE sequences of *ABCG2* promoter were generated by using a site-directed mutagenesis kit from Fast Mutagenesis System (TransGen Biotech, Beijing, China). Wild-type *ABCG2* promoter-luc was used as the template. Primers containing the mutant ARE sequences were used for PCR amplification of the mutant ABCG2 ARE binding site in the promoter, and then PCR products were digested with *Dpn*I for 1 h to cleave the wild-type promoter-luc template. Mutated nucleotides were verified by DNA sequencing. The primers used above are listed in Supplementary Table 7.

Analysis of luciferase activity was performed according to the manufacturer's protocol for the Dual-Luciferase Reporter System (Promega, Madison, WI, USA). GBC-SD and QBC-939 cells were co-transfected with the desired Firefly luciferase reporter plasmids and the Renilla luciferase construct (pRL-TK) used as the internal control. The normalized luciferase activity was expressed as a ratio of firefly luciferase to Renilla luciferase units.

2.16. Chromatin immunoprecipitation analysis and qPCR (ChIP-qPCR) analysis

ChIP analysis was used to determine the direct association of endogenous Nrf2 protein with the native ABCG2 promoter in GBC-SD cells by a SimpleChIP® Enzymatic Chromatin IP Kit (Cell Signaling, Danvers, MA, USA). Briefly, GBC-SD cells (1×10^7) were treated with 1% formaldehyde for 10 min to cross-link protein-DNA complexes, and reactions were quenched using 125 mM glycine for 5 min at room temperature. Then cells were lysed with SDS lysis buffer and chromatin was extracted and sonicated for 10 min using a Bioruptor Sonication (Diagnode, Liege, Belgium). After confirmation by agarose gel electrophoresis, the fragmented chromatin was precleared with BSA and protein A Sepharose Beads (Millipore Corporation, Billerica, MA, USA) at 4 °C for 2 h, prior to immunoprecipitation with anti-Nrf2 antibody (Cell Signaling Technology, Danvers, MA, USA) or rabbit control IgG antibodies overnight at 4 °C. The sepharose beads were extensively washed and eluted with SDS elution buffer, then were reverse cross-linked at 65 °C overnight, followed by purification of genomic DNA using the QIAquick PCR Purification Kit (Qiagen, Hilden, Germany) according to the manufacturer's protocol. Finally, target and nontarget regions were amplified by qPCR with a pair of primers specifically targeting the *ABCG2* promoter region that encompasses a Nrf2 response element. IgG included in the kit was used as a negative control for immunoprecipitation. A control primer set for *ABCG2* exon1 was used as a negative control for PCR. ChIP-qPCR primer sequences are listed in Supplemental Table 7. Two percent of chromatin before immunoprecipitation was saved as input, and ChIP data were presented as the percentage of input signal from three independent experiments.

2.17. Animal studies

Male 4 week-old athymic nude mice, SCID-beige mice, and immune-intact C57BL/6 mice were purchased from Shanghai Lab-Animal Research Center, and were quarantined, housed, and maintained in a specific pathogen-free environment in the animal barrier facility at Renji hospital, and were fed with normal chow diet. To generate xenografts, 1×10^6 GBC-SD or QBC-939 (sh-Con and sh-*NFE2L2*) cells were mixed 1:1 with Matrigel (BD Bio- sciences) and injected s.c. into the flank of each nude mice. For determining the effect of Nrf2 on tumor growth, chemosensitivity, efficacy of postoperative adjuvant chemotherapy (cisplatin; Sigma, St. Louis, MO, USA), mice were randomly assigned to 6 groups (sh-Con + Saline vs. sh-*NFE2L2* + Saline; sh-Con + cisplatin vs. sh-*NFE2L2* + cisplatin; sh-Con + surgery + cisplatin vs. sh-*NFE2L2* + surgery + cisplatin) for GBC-SD and QBC-939, until the tumors reached a measurable size of 0.5 cm in diameter. Six mice were used for each group. Cisplatin (6 mg/kg) was given to mice in the chemotherapy subgroup once every 9 days for 36 days, so as mice in the chemotherapy-combined surgery subgroup after subcutaneous tumor resection. Saline injection was used for the non-treatment groups (neither chemotherapy nor surgery). Tumor size was measured every 3 days by caliper from the time of palpable tumor formation, and tumors were weighed when mice were subjected to necropsy on 48th days for GBC-SD or 57th days for QBC-939. Tumor volume was calculated by the formula of length × width^2 × 0.5 [18]. Tumors were fixed in 4% formaldehyde and embedded in paraffin. Sections (4 μm thick) were stained with H&E in accordance with standard procedures. All animal procedures were performed according to national and international guidelines, and all studies were approved and supervised by the Animal Care and Use Committee of Shanghai Jiao Tong University.

2.18. Statistics

All cell assays were conducted at least 3 independent experiments. Statistical analyses were done using the IBM SPSS Statistics analysis software, version 19.0 (Chicago, IL, USA). Data are presented as the mean ± standard error of the mean (SEM) as indicated in the figure legends. *NFE2L2* mRNA and protein

expression and its correlation with *GPX4*, *CAT*, and *GSR* mRNA expression were assessed using Spearman's rank correlation coefficient, respectively. All other comparisons between groups were analyzed by unpaired 2-tailed Student's *t*-test or χ^2 test. A *P* value <.05 was considered statistically significant.

3. Results

3.1. Association of genotype of oxidative stress-related genes with OS is modified by adjuvant chemotherapy

In order to investigate whether OS pathway related variants are associated with BTC chemotherapy sensitivity, 66 genetic variants in 21 oxidative stress-related genes were selected and genotyped (Supplementary Table 1 and Supplementary Fig. 1) in 367 patients with or without chemotherapy (159 vs. 208). Four SNPs (*GPX4*_rs4807542; *GSR*_rs3779647, rs2978663 and rs8190996) with strong OS associations were identified in BTC chemotherapy treated group both by univariate and multivariate analysis, whereas these associations were not observed or mildly related in the non-chemotherapy group (Supplementary Table 2 and Supplementary Fig. 2). We then analyzed BTC subgroups, such as GBC and CC patients separately. In GBC patients treated with chemotherapy, rs4807542_AA/AG, rs3779647_CC, rs2978663_CC/CT, and rs8190996_GG/GA genotypes showed significantly better OS than their other counterparts, while these associations were not observed in the non-chemotherapy group (Fig. 1a, Supplementary Fig. 3, and Supplementary Table 3). In CC subgroup, we found that rs769217_CC/CT, rs3779647_CC, rs2978663_CC/CT, and rs2978662_GG/GA genotypes showed significantly better OS only in chemotherapy treated patients (Fig. 1a, Supplementary Fig. 4, and Supplementary Table 4). In addition, multivariate Cox regression analysis of interaction between each SNP (in the dominant model) and chemotherapy were investigated along with adjustment for the prognostic related factors identified in Supplementary Table 5 ($P < .05$), in GBC and CC group respectively. Interestingly, the interaction between the associated SNPs (*GPX4*_rs4807542; *CAT*_rs769217; *GSR*_rs8190996, rs3779647, rs2978663, and rs2978662) and chemotherapy had strong impacts on OS (Supplementary Table 6).

3.2. Functional SNPs alter expression of candidate genes

The molecular mechanism underlying the association between the polymorphisms in *CAT*, *GPX4*, as well as *GSR* and chemosensitivity in GBC and CC has not been investigated. Rs4807542 and rs769217 are synonymous variants located in the first exon of *GPX4* and the ninth exon of *CAT*, while the other 4 significant polymorphisms (rs8190996, rs3779647, rs2978663, and rs2978662) are in *GSR* intron (Supplementary Table 1). None of these SNPs result in alteration of amino acid sequence of protein products of candidate genes. To find out whether these associated SNPs are linked with change in gene expression, we inspected 2 cis-gene expression quantitative trait loci (cis-eQTL) databases from European Caucasian population [19,20] and found that rs4807542, rs769217, and rs3779647 correlated with the expression of CAT, GPX4, and GSR. No influence on gene expression was found with the 3 *GSR* intron located SNPs rs8190996, rs2978663, and rs2978662. Nevertheless, linkage disequilibrium (LD) analysis showed that they are linked with rs3779647 (rs8190996, D' = 0.91, $r^2 = 0.66$; rs2978663, D' = 0.99, $r^2 = 0.75$; rs2978662, D' = 0.96, $r^2 = 0.15$; in Chinese Han BTC samples) (Supplementary Fig. 5). In addition, after conditioning on rs3779647, none of the other *GSR* SNPs retained a significant association ($P > .05$, data not shown), indicating that rs3779647 might be an independent SNP that is associated with chemosensitivity in BTC.

SNPs outside coding region may regulate gene expression through effect on RNA splicing, transcription factor binding, and DNA methylation [21]. To investigate if the candidate SNPs in *CAT*, *GPX4* and *GSR* are involved in such mechanisms, a 300 bp region surrounding the 3 SNPs were analyzed for potential regulatory elements by inspecting the UCSC Genome Browser. We found that rs4807542 is located within a transcription factor binding site, whereas rs3779647 and rs769217 are located in a DNase I hypersensitive sites, based on ENCODE database [22] (Supplementary Fig. 6).

In order to validate a regulatory role of these candidate SNPs, we analyzed the expression of CAT, GPX4, GSR, and Ki-67 in 36 GBC and 52 CC tissue samples, respectively. Genotypes of the 3 SNPs were also examined. Consistent with our hypothesis, rs4807542_A, rs769217_C, and rs3779647_C alleles, which were associated with better prognosis in GBC or CC patients who received chemotherapy, exhibit higher levels of GPX4, CAT, and GSR and lower levels of Ki-67 in the tumor tissues, respectively (Fig. 1c–f, Supplementary Fig. 7).

3.3. GPX4, CAT and GSR regulate chemosensitivity through ABCG2

Recently, regulatory SNPs have come into sight [23]. Our results suggest that the SNPs in *GPX4*, *CAT* and *GSR* possibly execute their effect on chemosensitivity by influencing expression of their respective genes. To confirm the functional significance of these SNPs and to elucidate the precise mechanism on chemosensitivity, and their relation with gene expression, GPX4, CAT and GSR were knocked down or overexpressed in GBC (GBC-SD) and CC (QBC-939) cell lines respectively (Fig. 2a–b). Consistently, increased GPX4, GSR or CAT expression promoted cisplatin and doxorubicin-induced antitumor effect as evidenced by reduced IC50 (Fig. 2c–d). Annexin V staining and FACS analysis further revealed that the cell apoptotic rate increased in GPX4, GSR or CAT-upregulated cells upon cisplatin treatment (Supplementary Fig. 8). On the contrary, cells were more resistant to cisplatin-induced death with reduced GPX4, CAT, or GSR expression (Supplementary Fig. 8). To test whether GPX4, CAT, and GSR contribute to the proliferation of BTC cells, we also determined the growth profiles in cultured cells and observed that overexpression of GPX4, CAT, and GSR, inhibit proliferation of GBC-SD and QBC-939 cells (Supplementary Fig. 9).

Cancer cells exploit various mechanisms against chemotherapy agents, such as, reducing drug accumulation to attenuate DNA damage, or inhibiting the damage signaling to the apoptotic machinery [24]. ATP-binding cassette (ABC) proteins belong to one of the largest families of membrane proteins. They are involved in the regulation of transportation of hydrophobic compounds across cellular membranes. The expression of ABC proteins is regulated in response to many endogenous and xenobiotic compounds, including cisplatin and doxorubicin [25]. Among the 50 members, ABCB1, ABCC1, ABCC2, ABCC3 and ABCG2 have been constantly reported to be correlated with chemotherapy efficacy [26]. To find out whether these genes are involved in chemosensitivity caused by *GPX4*, *CAT* and *GSR* variants, ABCB1, ABCC1, ABCC2, ABCC3 and ABCG2 expression level were determined in GPX4, CAT or GSR knocked down GBC-SD and QBC-939 cell lines respectively. Interestingly, the expression of other 4 ABC members was not significantly changed except ABCG2 (Supplementary Fig. 10 and Fig. 2a–b). Decrease of GPX4, CAT or GSR expression obviously up-regulated both mRNA and protein levels of ABCG2 in GBC-SD and QBC-939 cell lines (Fig. 2a–b). Conversely, their overexpression reduced ABCG2 expression (Fig. 2a–b). All the above in vitro results prompted us to hypothesize that the variations in these 3 oxidative stress-related genes may influence chemotherapeutic effects by regulating ABCG2 expression. To further confirm this result, ABCG2 expression was examined in previously mentioned 36 GBC and 52 CC tissue samples.

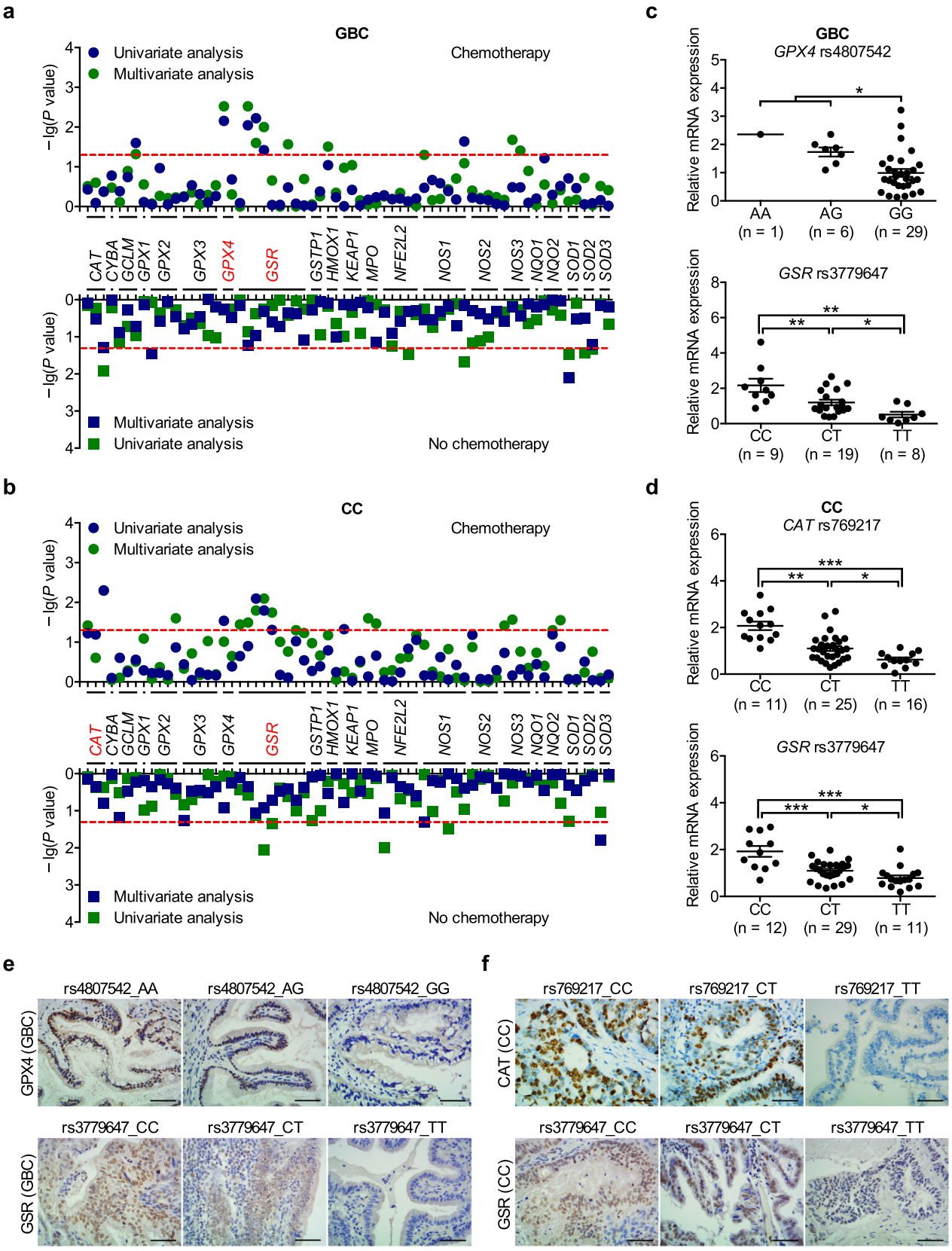

Fig. 1. Identification and functional investigation of susceptibility SNPs associated with chemosensitivity in BTC. (a and b) Association analysis of oxidative stress-related gene polymorphisms and OS in GBC (a) and CC (b) patients. The 66 SNPs from 21 oxidative stress-related genes are represented on the X-axis. On the Y-axis, statistical significance is expressed as -$\log_{10}$ *P* value. The red horizontal line represents the threshold *P* value of 0.05. The genes depicted as red italics contain SNPs that were strongly associated with OS with adjuvant chemotherapy. (c and d) GPX4, CAT, and GSR mRNA expression are strongly associated with genotypes of rs4807542 (c, upper), rs769217 (d, upper), and rs3779647 (c and d, lower) in 88 BTC samples respectively. Bar, SEM. (e and f) Representative IHC images stained for GPX4 and GSR were stratified by genotypes of rs4807542 (e, upper) and rs3779647 (e, lower) in 36 GBC specimens, and CAT and GSR were stratified by genotypes of rs769217 (f, upper) and rs3779647 (f, lower) in 52 CC specimens, respectively. Original magnification, × 400; scale bars: 50 μm. $^{*}P < .05$, $^{**}P < .01$, $^{***}P < .001$, Student's *t*-test. (For interpretation of the references to colour in this figure legend, the reader is referred to the web version of this article.)

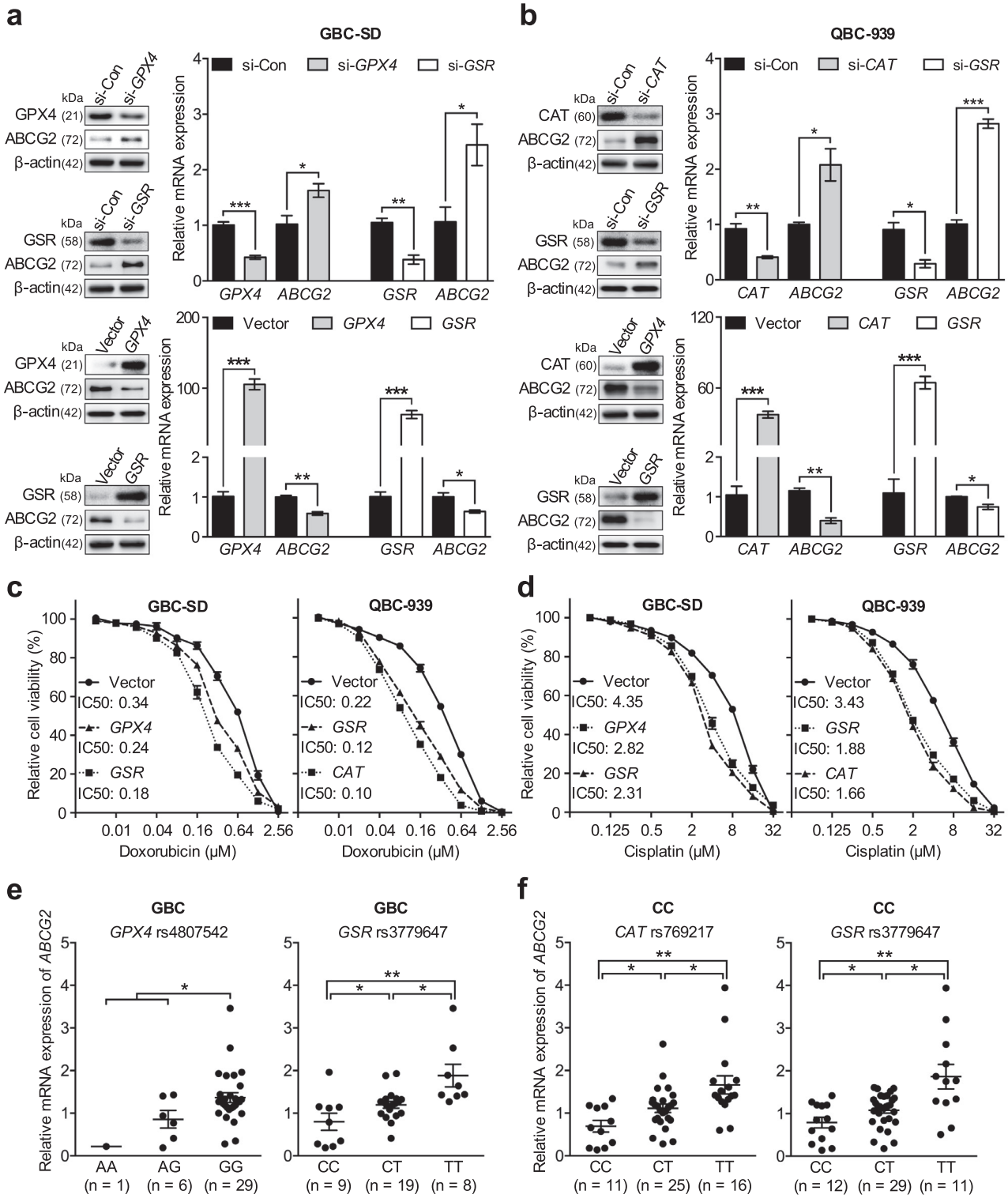

Fig. 2. GPX4, CAT, and GSR regulate ABCG2 expression and cisplatin resistance in BTC cells. (a and b) Immunoblot and qPCR analysis of ABCG2 expression in response to downregulation or overexpression of GPX4 and GSR in paired GBC-SD (a), and in response to downregulation or overexpression of CAT and GSR in paired QBC-939 (b). $n = 3$; Bar, SEM. (c and d) GBC-SD and QBC-939 cells were transfected with *GPX4*, *GSR* and *CAT*, *GSR* or empty vector, followed by treatment with a concentration-gradient of cisplatin (c) or doxorubicin (d) for 48 h. Cell survival was determined using the MTS assay. $n = 4$; Bar, SEM. (e and f) Levels of ABCG2 mRNA stratified by rs4807542, rs769217, and rs3779647 genotype in GBC (a) and CC (b) tissues. $^{*}P < .05$, $^{**}P < .01$, $^{***}P < .001$, Student's *t*-test.

We found that ABCG2 expression is not only correlated with *GPX4*, *CAT* and *GSR*'s genotype, but also is correlated with their mRNA level (Fig. 2e–f, Supplementary Fig. 11).

3.4. GPX4, GSR and CAT regulate Nrf2 and ABCG2 via ROS

Oxidative stress caused by elevated levels of ROS has been observed in almost all cancers, where they contribute to disease development and progression [27]. GPX4, CAT and GSR proteins actively participate in detoxifying ROS and thus serve as crucial regulators of cellular ROS state [28]. However, whether reduced expression of GPX4, CAT and GSR can affect cellular ROS and associate with chemoresistence has not been investigated. A ROS-sensitive dye, 2′,7′-dichlorodihydrofluorescein diacetate (H2DCFDA), was used to determine cellular ROS levels in GBC-SD and QBC-939 cells respectively. An increased production of cellular ROS was observed in GPX4, CAT, or GSR knockdown cells, however ROS rapidly decreased in GPX4, CAT, or GSR overexpressed cells (Fig. 3a–b, Supplementary Fig. 12).

Increasing evidences in recent years have suggested that ROS is not just a mutagenic agent in cancer development but has additional roles to play. Precise regulation and a critical balance of intracellular ROS levels are required for cancer cell function, growth, and survival. The Nrf2-antioxidant response element (ARE) pathway is an important redox-sensing apparatus that is involved in tumorigenicity. Nrf2, a transcription factor, prevents cell transformation from nonmalignant to malignant [29], and regulates ROS level through transcriptional activation of detoxifying and antioxidant enzymes. But on the other hand, Nrf2 can also protect the tumor from OS and chemotherapy-induced cytotoxicity [30]. We hypothesize that ROS production induced by *GPX4*, *CAT* and *GSR* variants may stimulate Nrf2 expression. Therefore, to find out whether Nrf2 is involved in chemoresistance conferred by *GPX4*, *CAT* and *GSR* variants, we examined mRNA and protein levels of Nrf2 in genotyped GBC and CC samples along with GPX4, CAT and GSR expression. Interestingly, we found that Nrf2 protein level correlates well mRNA level of GPX4, CAT and GSR, but not Nrf2 mRNA expression level (Fig. 3c–d, Supplementary Fig. 13). We further confirmed these results in GBC-SD and QBC-939 cell lines. Silencing of *GPX4*, *CAT* or *GSR* gene expression upregulated NQO1 expression, a ROS state indicative gene, both at protein and mRNA level (Fig. 3e–f). Increased Nrf2 protein was also observed, although the mRNA level did not change significantly (Fig. 3e–f). Conversely, GPX4, CAT and GSR overexpression resulted in decrease of NQO1 and Nrf2 protein level (Fig. 3e–f). Moreover, GPX4, CAT and GSR-overexpressing cells displayed substantially diminished ARE luciferase activity compared with control cells (Supplementary Fig. 14).

To further elucidate the precise relationship among reduced GPX4, CAT and GSR expression, increased cellular ROS and Nrf2, and ineffective chemotherapy induced by *GPX4*, *CAT* and *GSR* variants, we first examined the expression of Nrf2 and ABCG2 in GPX4, GSR or CAT deficient GBC-SD and QBC-939 cell lines treated with *N*-acetyl-cysteine (NAC), a cellular ROS scavenger. Increased Nrf2, NQO1 and ABCG2 expression caused by GPX4, GSR or CAT deficiency were reversed by NAC treatment (Fig. 3g–j). Moreover, NAC supplemented inhibited cell proliferation and increased cisplatin cytotoxic effect by facilitating cell apoptosis (Supplementary Figs. 15–16). Thus we conclude that Nrf2 and ABCG2 expression induced by reduced expression of GPX4, GSR or CAT is ROS dependent.

3.5. Nrf2 enhance chemoresistance by promoting ABCG2 expression

In order to find out the role Nrf2 played in BTCs, protein level of Nrf2 was analyzed in BTC samples, and compared with their survival rate. Increased Nrf2 protein expression was found to be exclusively associated with poor prognosis in both GBC and CC patients administrated with postoperative adjuvant chemotherapy (Fig. 4a–b). To further assess the contribution of Nrf2 to cisplatin and doxorubicin resistance, Nrf2 in GBC-SD and QBC-939 cells was knocked down with NFE2L2 (Nrf2 gene name) shRNA, and cell sensitivity was determined. Nrf2 depletion promoted cisplatin or doxorubicin-induced cell killing, with 2.3–2.6-fold reduction of IC50 (Supplementary Fig. 17). Furthermore, elevated apoptosis rate and reduced cell proliferation were observed in Nrf2 depleted GBC-SD and QBC-939 cell lines. Conversely, Nrf2 overexpression or addition of its activator, tertiary-butylhydroquinone (t-BHQ), exhibited the opposite effect, enhancing resistance to cisplatin and inducing cell proliferation in both cell lines (Fig. 4c–d, Supplementary Fig. 18).

Attenuation of Nrf2 expression in many cancer cells leads to a decline in ABCG2 mRNA and protein levels [17]. Nrf2 has been suggested to utilize various ways in resisting chemotherapy effect in BTC [31]. But the precise mechanism involved is poorly understood. To clarify how ABCG2 is regulated by Nrf2, we first examined mRNA levels of 5 chemoresistance-related genes in GBC-SD and QBC-939 cell lines, in which Nrf2 was knocked down. Nrf2 depletion lead to down regulation of ABCG2 expression, whereas, expression of other 4 genes ABCB1, ABCC1, ABCC2 and ABCC3 was not affected (Fig. 4e–f, Supplementary Fig. 19). In addition, Nrf2 overexpression increased ABCG2 mRNA and protein level in both GBC-SD and QBC-939 cell lines (Fig. 4e–f). Decreased ABCG2 expression on cell membrane after Nrf2 knockdown was also confirmed by immunofluorescence analysis (Fig. 4g–h). No effect was observed on GPX4, GSR or CAT mRNA and protein amounts (Supplementary Fig. 20). All these results suggest that Nrf2 may specifically target ABCG2 expression in orchestrating cancer chemoresistance.

3.6. Nrf2 directly mediates GPX4, CAT and GSR-induced ABCG2 downregulation

In order to identify whether Nrf2 directly mediates ABCG2 upregulation induced by GPX4, CAT and GSR depletion, ABCG2 expression was analyzed in GBC-SD and QBC-939 cells, in which Nrf2 expression was attenuated in GPX4, CAT or GSR knocked-down background. Reduced Nrf2 expression abolished the increase in both mRNA and protein level of ABCG2 observed with GPX4, CAT or GSR depletion. (Fig. 5a–d). To investigate if there is a direct influence of Nrf2 on the promoter of the ABCG2 gene, a 1-kb DNA segment located upstream of the ABCG2 transcription initiation site was introduced into a luciferase reporter construct, and regulation of luciferase activity was examined in GBC-SD and QBC-939 cells. GPX4, CAT or GSR depletion induced Nrf2 dependent increase of luciferase activity (Fig. 5e–f). In silico analysis of ABCG2 promoter identified a putative ARE located at −431 to −420 bp upstream of the ABCG2 transcription start site, and it exhibits strong sequence similarity to the canonical Nrf2-binging site [17]. Accordingly, we generated a mutant ABCG2 promoter reporter construct harboring three point mutations in the center of the putative Nrf2-response element (Fig. 5g). This ABCG2 promoter reporter mutant construct was introduced into GBC-SD and QBC-939 cell lines and analyzed. In contrast to its wild type counterpart, the mutant promoter eliminated Nrf2 mediated increase of luciferase activity (Fig. 5h–i).

To confirm the direct binding of Nrf2 on the ABCG2 promoter in vitro, we extended these studies by performing chromatin immunoprecipitation analysis (ChIP) analysis. We isolated chromatin-nuclear protein complexes immunoprecipitated with anti-Nrf2 antibody from GBC-SD cells,and analyzed it by qPCR using primers that specifically encompass the putative Nrf2-response element in the ABCG2 promoter. The physical association of Nrf2 with the ABCG2 promoter sequences was detected, while limited signals

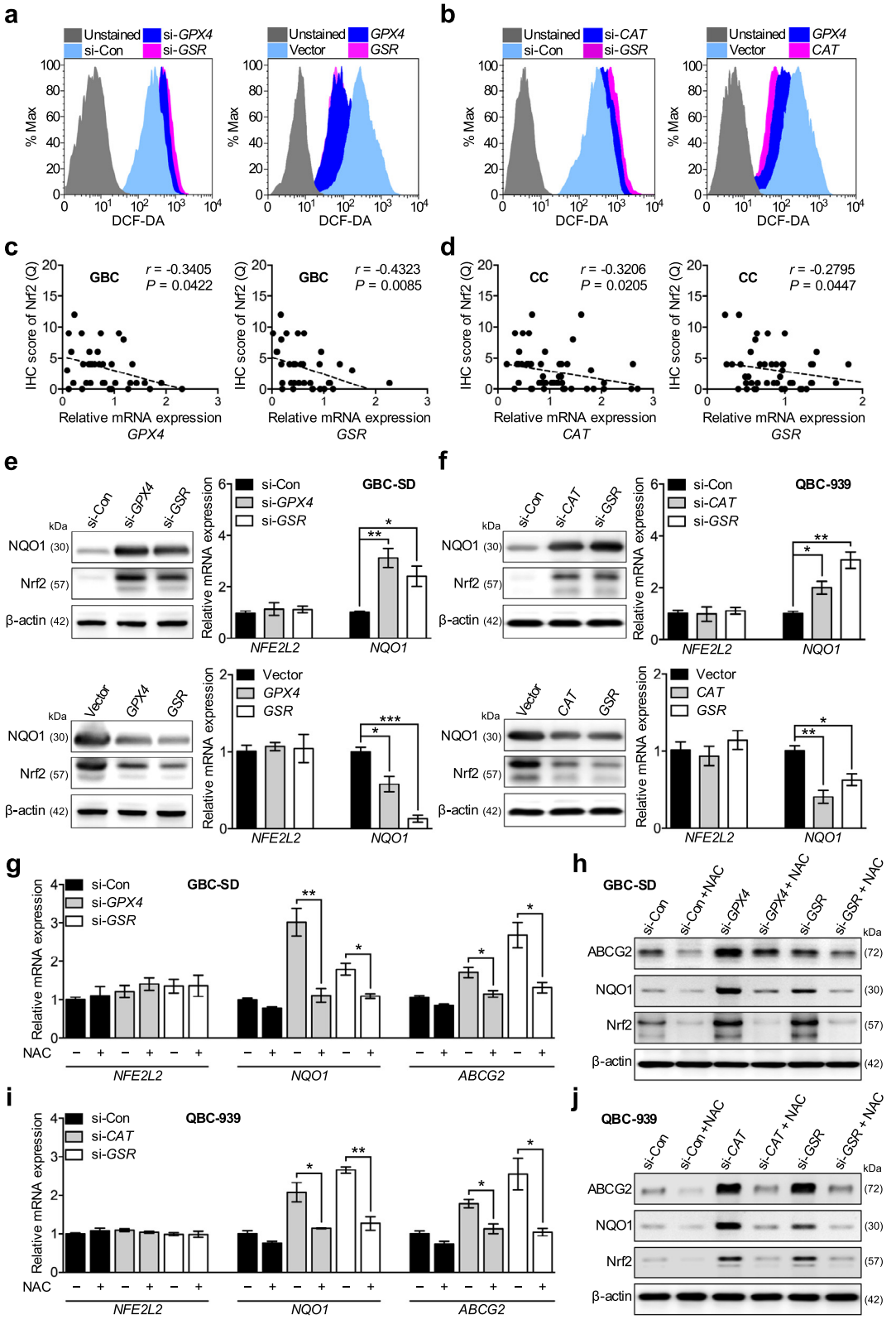

Fig. 3. GPX4, CAT, and GSR regulate Nrf2 protein expression through ROS. (a and b) Representative FACS profile of ROS levels, which was measured by H2DCFDA staining, in GBC-SD (a) and QBC-939 (b) when GPX4, CAT, or GSR was overexpressed or knockdown. (c and d) Analysis of correlation between the protein level of Nrf2 and the mRNA level of GPX4 (c, left) or GSR (c, right) was performed in 36 GBC tissues, and the mRNA level of CAT (d, left) or GSR (d, right) was performed in 52 CC tissues. Spearman's correlation was used. (e and f) Immunoblot and qPCR analysis of Nrf2, and it target NQO1 from GBC-SD transfected with scrambled siRNA (si-Con) or siRNA (si-*GPX4* and si-*GSR*) and empty vector, *GPX4*, or *GSR* (e), and from QBC-939 transfected with si-Con or siRNA (si-*CAT* and si-*GSR*) and empty vector or *CAT* or *GSR* (F). $n = 3$; Bar, SEM. (g and i) qPCR analysis of NFE2L2, NQO1 and ABCG2 expression in GBC-SD (g: si-Con, si-*GPX4* and si-*GSR*), and in QBC-939 (i: si-Con, si-*CAT* and si-*GSR*) cells cultured in standard media supplemented with or without 10 mM NAC. n = 3; Bar, SEM. (h and j) Immunoblots of Nrf2, NQO1 and ABCG2 protein in GBC-SD (h: si-Con, si-*GPX4* and si-*GSR*), and in QBC-939 (j: si-Con, si-*CAT* and si-*GSR*) cells incubated with or without 10 mM NAC. $^{*}P < .05$, $^{**}P < .01$, $^{***}P < .001$, Student's *t*-test.

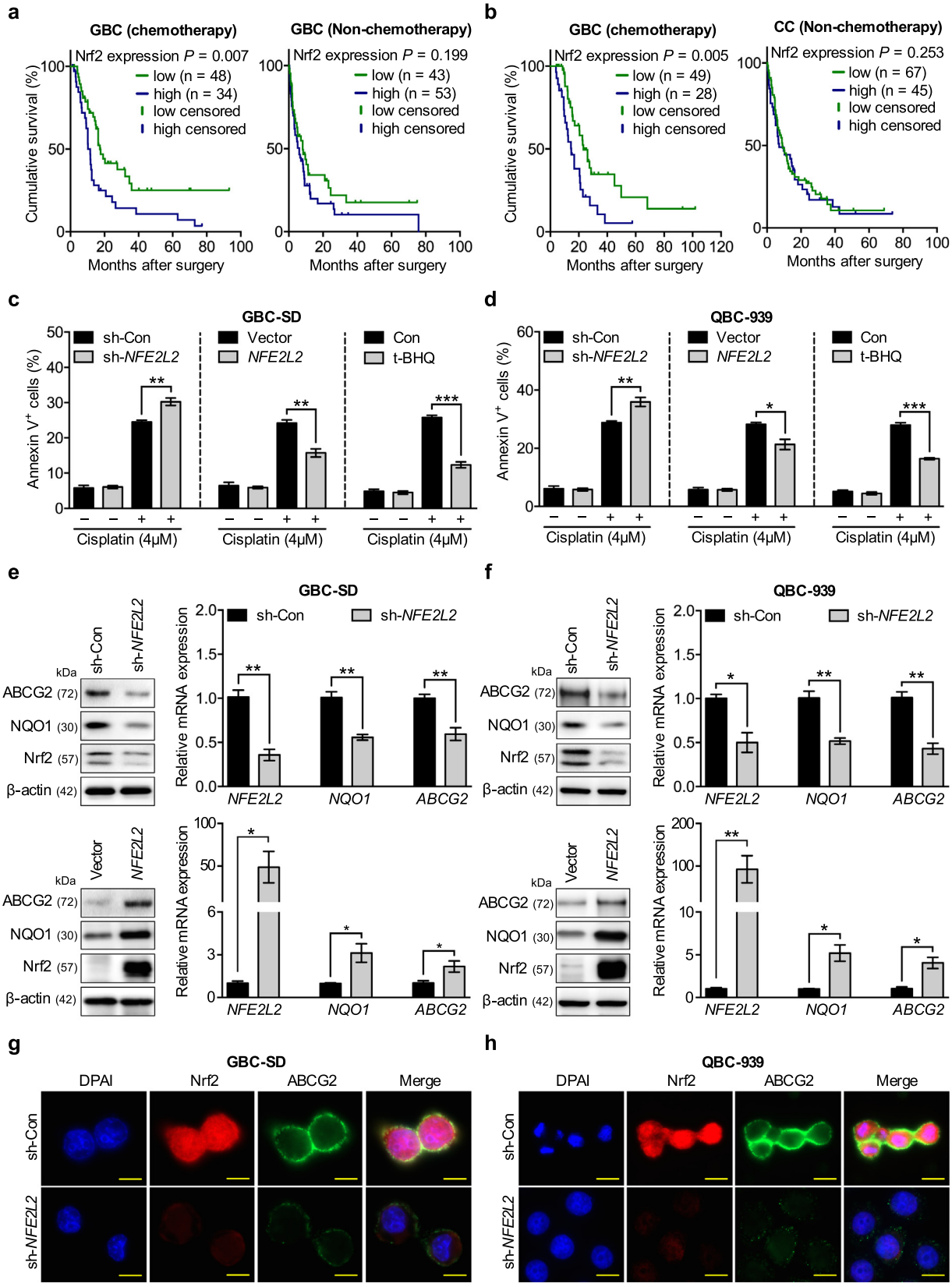

Fig. 4. Nrf2 promotes chemoresistance by inducing expression of ABCG2. (a and b) Kaplan-Meier curves of OS was plotted as a function of Nrf2 protein levels in GBC (a) and CC (b) patients, who had or had not received adjuvant chemotherapy. Nrf2 high, IHC score > 3; Nrf2 low, IHC score ≤ 3. The *P* value was calculated by a log-rank test. (c and d) Apoptosis analysis of GBC-SD (c) and QBC-939 (d) Cells in response to cisplatin when NFE2L2 was stably knockdown, or overexpressed, or when the cells were treated with Nrf2 agonists (t-BHQ 50 μM). $n = 4$; Bar, SEM. (e and f) Immunoblot and qPCR analysis of NQO1 and ABCG2 from paired GBC-SD (e up: sh-Con and sh-*NFE2L2*; e down: vector and *NFE2L2*) and QBC-939 (f up: sh-Con and sh-*NFE2L2*; f down: vector and *NFE2L2*). n = 3; Bar, SEM. (g and h) Immunofluorescence analysis of ABCG2 (green) and Nrf2 (red) from paired GBC-SD (g) and QBC-939 (h). DAPI (blue) serve as markers for nuclei. Representative images are shown. Original magnification, × 400; scale bars: 5 μm. $^{*}P < .05$, $^{**}P < .01$, $^{***}P < .001$, Student's *t*-test. (For interpretation of the references to colour in this figure legend, the reader is referred to the web version of this article.)

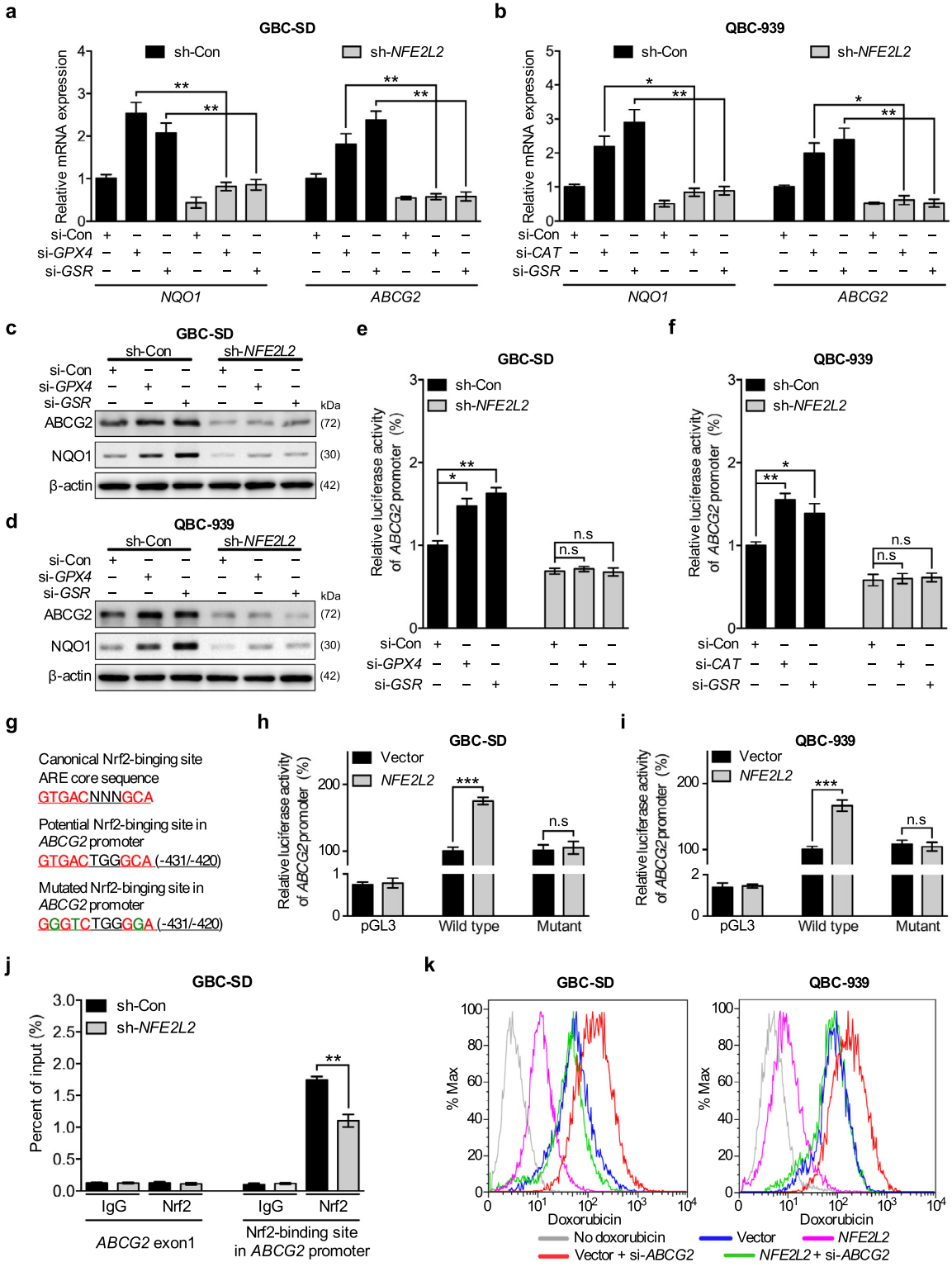

Fig. 5. GPX4, CAT, and GSR regulate chemosensitivity through Nrf2-mediated ABCG2 expression. (a and b) qPCR analysis of ABCG2 and NQO1 mRNA expression in paired GBC-SD (a) and QBC-939 (b) cells transfected with or without siRNA of *GPX4*, *GSR*, *CAT*. n = 3; Bar, SEM. (c and d) Immunoblots of ABCG2 and NQO1 in paired GBC-SD (c) and QBC-939 (d) cells that expressed *GPX4*, *GSR*, or *CAT* targeting siRNAs or a scrambled siRNA. (e and f) ABCG2-promoter luciferase assay in paired GBC-SD (a) and QBC-939 (b) cells that were transfected with or without siRNA of *GPX4*, *GSR*, *CAT*. n = 3; Bar, SEM. (g) The canonical sequence of the Nrf2-binding site (top, red), a potential Nrf2-binding site at -431 bp to -420 bp in the proximal promoter region of the human ABCG2 gene (middle, red), and introduced point mutations (bottom, green) used to inactivate the potential ABCG2-binding site are shown. (h and i) Determination of luciferase activity using vector only, wild type or mutant *ABCG2* promoter in different pairs of GBC-SD (h) and QBC-939 (i) cells. (j) ChIP analysis of paired GBC-SD (sh-Con and sh-*NFE2L2*) cells immunoprecipitated by anti-Nrf2 or IgG antibody followed by qPCR using 2 primer sets for the Nrf2-binding site in the *ABCG2* promoter or *ABCG2* exon 1, respectively. Data represent the percent of input. n = 3; Bar, SEM. (k) Doxorubicin efflux of paired GBC-SD (left) and QBC-939 (right) cells were detected by FACS. $^{*}P < .05$, $^{**}P < .01$, $^{***}P < .001$, Student's *t*-test. (For interpretation of the references to colour in this figure legend, the reader is referred to the web version of this article.)

were detected from the negative controls, in which either nonspecific IgG antibody was used in the immunoprecipitation step or the ABCG2 exon 1 was probed in order to confirm the targeting specificity of the primer set used in qPCR. The physical association of Nrf2 with the ABCG2 promoter sequence was reduced after depletion of Nrf2 (Fig. 5j). Moreover, we found that the knockdown of GPX4, GSR or CAT enhanced Nrf2-binding at the ABCG2 promoter, as shown by ChIP analysis (Supplementary Fig. 21). These results further supported our finding that upregulation of ABCG2 expression is Nrf2-dependent.

ATP-binding cassette transporters such as ABCG2, have been implicated in the multidrug resistance of cancer cells through enhancing drug efflux. In GBC-SD and QBC-939 cells, upregulation of Nrf2 to evade apoptosis can be blocked by ABCG2 knockdown (Supplementary Fig. 22). Furthermore, the effects of Nrf2 in drug uptake were determined by measuring intracellular content of the autofluorescent drug doxorubicin. Nrf2 overexpression significantly decreased drug accumulation in GBC-SD and QBC-939 cells, whereas ABCG2 knockdown significantly decreased Nrf2-mediated drug efflux (Fig. 5k, Supplementary Fig. 23).

3.7. Nrf2 is the key element for growth and chemoresistance of BTC xenografts

We further analyzed the effect of Nrf2 on chemotherapy efficacy in a xenograft model that was treated with cisplatin in vivo. After male nude mice were implanted subcutaneously with GBC-SD or QCB-939 expressing *NFE2L2*-targeting shRNA, they presented with slower rate of tumor growth than controls (Fig. 6a and c). In chemotherapy group and postoperative chemotherapy group, cisplatin (6 mg/kg) was administered once every 9 days for 36 days. Similar to the chronic treatment, this short-term cisplatin treatment also inhibited the growth of all xenografts in chemotherapy group, with Nrf2-depleted tumors exhibiting a less progressive growth dynamics and more significant tumor inhibition following treatments (Fig. 6a and c). Strikingly, we found that in postoperative chemotherapy group, stable knockdown of Nrf2 in GBC-SD and QCB-939 cells nearly eliminated tumor recurrence, in sharp contrast to tumor recurrence in mice inoculated with the control cells (Fig. 6a and c). As a comparison, we analyzed the protein expression patterns of select markers in GBC-SD and QBC-939 xenograft tumors by IHC (Fig. 6b and d, Supplementary Fig. 24). Ki-67 and ABCG2 staining of tumor specimens revealed significantly decrease of Ki-67$^+$ and ABCG2$^+$ cells in the Nrf2-knockdown GBC-SD and QBC-939 tumors (Fig. 6b and d). Moreover, Nrf2-knockdown xenograft tumors showed a higher rate of apoptosis than control group by TUNEL staining in GBC and QBC-939 chemotherapy groups (Fig. 6b and d).

3.8. Predictive value of polymorphisms in disease progression

Despite that the effect of a single SNP could be minor, the combined effect of multiple SNPs could be important for disease progression and outcome. To evaluate the combined effect of these functional variants in oxidative stress-related genes and Nrf2 expression level, the previously described combined "score" system was also used in our study [32]. As it showed that, risk factors (*GPX4*, *CAT* and *GSR* genotype or Nrf2 expression) were assigned "0" and protective factors were assigned "1". Thus, each patient was given an oxidative stress-related score ranging from 0 to 5. Then both GBC and CC patients were divided into 2 groups according to their scores (score 0–2, and score 3–5). The combined genetic score predicted cumulative survival rate in the chemotherapy group (Fig. 7a and c) but not in the non-chemotherapy group (Supplementary Fig. 25). We then evaluated the predictive value of genetic score for disease progression in patients who received chemotherapy. Oxidative stress-related score was added in clinical score to create total score. ROC analysis showed an AUC (0.72, 0.80, and 0.86 in GBC, and 0.67, 0.78, and 0.83 in CC) and Youden-index (0.38, 0.47, and 0.62 in GBC, and 0.24, 0.45, and 0.49 in CC) for the clinical model, oxidative stress-related model, and total model, respectively (Fig. 7b and d). In addition, the total model had a better AUC compared with clinical model in GBC and CC patients ($P_{GBC} = 0.043$ and $P_{CC} = 0.034$ for AUC comparison), indicating an improved prediction capability for postoperative chemotherapy efficacy by adding oxidative stress-related factors to clinical factors in the prediction model.

4. Discussion

Chemoresistance of BTC has been an unresolved issue for a long time [31,33], and a molecular understanding is critically needed. It has been suggested that cellular oxidative status can affect chemosensitivity [8,9], but how ROS level is regulated and whether host genetic factors also participate in its regulation and thus influence therapeutic effect of BTC has never been investigated. Alterations on a molecular level defining these differences in behavior and potential therapeutic targets are still inadequately defined. Yet, personalized therapy for BTCs is dependent on a better understanding of the driver genetic aberrations for each subtype of BTC [34]. Much success has been made in identifying genetic variants associated with common diseases using GWAS [4]. Recent endeavors have been carried out to figure out how these associated genetic variants execute their function under diverse circumstances, which would potentially facilitate their translation into clinical practice [35]. In this study, in order to find out the role of oxidative stress-related genes variants in biliary tract cancer (BTC) chemoresistance, 66 genetic variations of 21 oxidative stress-related genes were examined in 178 GBC and 189 CC patients and their association with overall survival (OS) were analyzed according to chemotherapy treatment received or not. Three novel genetic variants from *CAT*, *GPX4*, and *GSR* were found correlated with chemotherapy efficacy among BTC patients. Moreover, tight correlations between the 3 variants and their respective expression levels were found in human BTC specimens. CAT, GPX4, and GSR are all critical surveillance molecules regulating cellular ROS, and their variations specifically influence the prognosis of chemotherapy treated patients. We suggest that the function mediated by such genetic variants, which induced gene expression variation may be minor or could be substituted by other genes under steady state. However, when drugs, mostly alkylating agents, are added, they could induce an oxidative burst pressure on cell [36]. At this time, there would be an urgent need of these antioxidant genes to execute functions, the genetic variants in these genes so caused no sufficient protein generation would be deleterious. Moreover, since many anti-tumor drugs are ROS stimulating agents, cautiously considered and follow up should be implemented when such drugs are given to patients carrying specific oxidative stress-related variants.

Helped by in vitro experiment, we found that knock down *GPX4*, *CAT* and *GSR* in BTC cell lines, which mimic the effect of variants on expression, promoted cancer cell proliferation and chemoresistance through elevating ROS levels and subsequently activating Nrf2 related pathways. Increase of Nrf2 is capable of accelerating ABCG2 transcription, which in turn enhances drug efflux from BTC cells. ROS is a double-edged sword and multi-hand player in cancer. Original researches have been focused on its mutagenic effect and capability of influencing cancer cell proliferation and malignant transformation [37]. In recent years, increasing evidences have suggested that cellular ROS level is also related with therapeutic efficacy [8,9,38]. For example, Nrf2 repression promotes the antitumor effect of 5-fluorouracil and gemc-

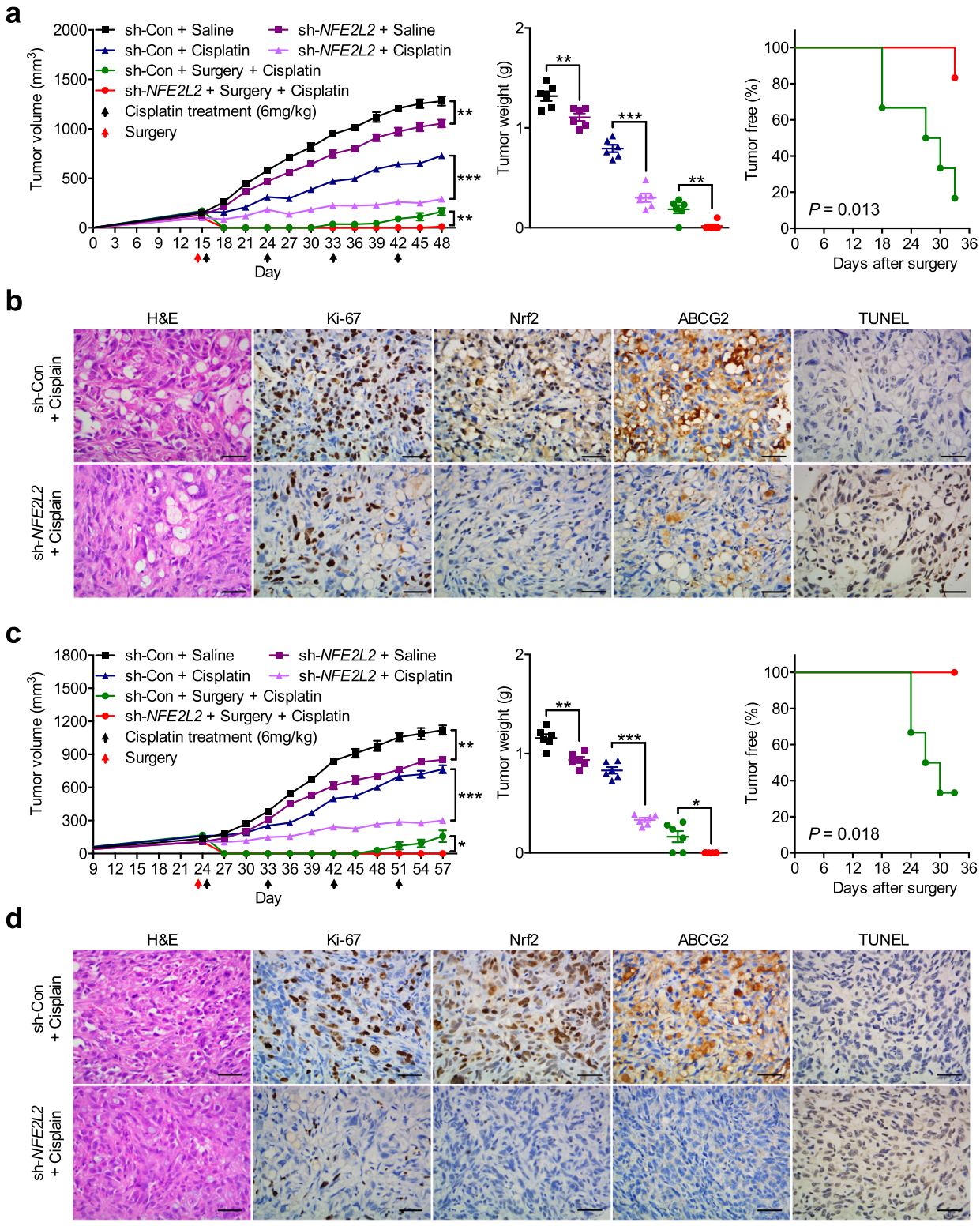

Fig. 6. Nrf2 is the key element for growth and chemoresistance of BTC xenografts. (a and c) GBC-SD or QBC-939 cells stably expressing *NFE2L2*-targeting shRNA (sh-*NFE2L2*) or scrambled shRNA (sh-Con) were injected into the flank of athymic nude mice s.c. ($n = 6$ mice for each group) to create tumor xenografts. After tumors were about 5 mm in diameter, the first paired mice group was treated with saline, the second was treated with cisplatin (6 mg/kg), and the third was combined radical surgery and cisplatin (6 mg/kg) treatment. The chemotherapy was given once every nine days for 1 month. Tumor growth was determined by measurement of tumor volume, tumor weight, and the frequency of tumor formation. Tumor growth curves (left), tumor weigh (middle), and tumor-free percentages (right) at the indicated times were plotted. n = 6; Bar, SEM. (b and d) H&E, TUNEL, and IHC analysis of Ki-67, Nrf2, and ABCG2 expressions in tumor (b: GBC-SD; d: QBC-939) xenografts of the second paired mice groups. Representative images from 6 separate samples are shown. Original magnification, × 400; scale bars: 50 μm. $^{*}P < .05$, $^{**}P < .01$, $^{***}P < .001$, Student's *t*-test.

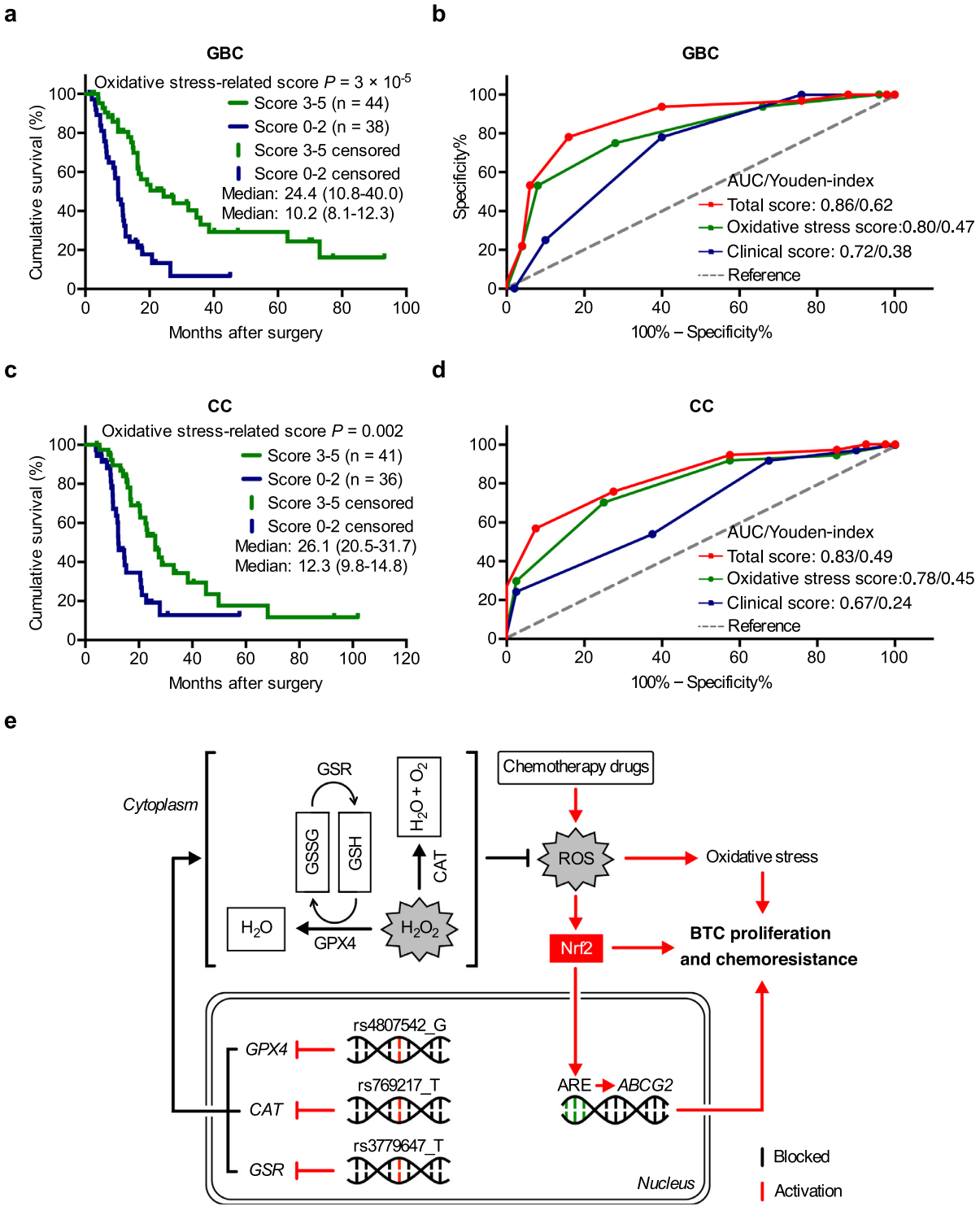

Fig. 7. Oxidative stress-related factors improve the prediction of chemotherapy efficacy in BTC patients. (a and c) Effect of oxidative stress-related score (0–2 vs. 3–5) on OS in GBC (a) and CC (c) patients treated with adjuvant chemotherapy. *P* value was calculated by log-rank test. (b and d) ROC curves assessing the discriminatory ability among total model, oxidative stress-related model, and clinical model for prediction of progression in GBC (b) and CC (d) patients who received chemotherapy. The total model contains oxidative stress-related score and clinical score. $P = .043$ (GBC) and $P = .034$ (CC) for AUC comparison between total model and clinical model. (e) Schematic model for how *GPX4*, *CAT*, and *GSR* polymorphisms regulate BTC proliferation and chemoresistance through crosstalk with ROS-activated Nrf2-ABCG2 signaling pathway. Variants in *GPX4*, *CAT*, and *GSR* gene can decrease their expression and induce generation of intracellular ROS levels. Stimuli, such as chemotherapy drugs, can exacerbate production of ROS, which can induce DNA damage and cancer evolution by oxidative stress. Together, ascension of ROS mediates the activation of Nrf2 signaling, which results in the activation of nuclear ABCG2 expression, and further in concert drive BTC proliferation and chemoresistance.

itabine on cholangiocarcinoma cells [39,40]. Several compounds like Dioscin, Metformin, Curcumin have been found capable of modulating the chemisesitivity of BTC through ROS related pathway [41–43]. However, the evidence for the relationship between ROS and chemosensitivity is sometimes contrary and there is still no consensus regarding whether increasing or decreasing ROS is beneficial for cancer chemotherapy. Hence, our study suggested that SNP analysis of tumor specimen might also be considered and could give hints for chemotherapy efficacy in patients with biliary tract cancer in future.

In conclusion, our results indicate that those seemingly minor genetic variations should not be ignore, on the contrary, they could be instructive for selecting chemotherapy according to patients' genetic information in the near future. Last but importantly, further validation of our scoring system by an extern patient group in the future would be helpful in achieving personalized treatment among BTC patients.

Funding sources

This work was supported by the National Science Foundation of China (81802424, 81773184, and 81803014), Foundation of Shanghai Shen Kang Hospital Development Center (16CR2002A and 16CR3028A), Innovative research team of high-level local universities in Shanghai (2018, JW), and Shanghai Outstanding Academic Leaders Plan (2016, JW). The funders had no role in study design, data collection and analysis, decision to publish, or preparation of the manuscript.

Author contributions

J.W. and R.-M.Y. designed and supervised the study, analyzed the data and wrote the paper. M.Z., H.W., S.-W.X, and L.-H.Y. performed the experiments, analyzed the data, performed the animal studies and statistical analysis. W·C, S.-X.Z., H·S, and Q.L provided the BTC patient samples. J.W. and R.-M.Y. edited and reviewed the manuscript. All authors read and approved the final version of the paper.

Declaration of Competing Interest

The authors declare no conflicts of interest that pertain to this work.

Acknowledgements

We are indebted to the staff, patients and all other individuals involved in this study for their dedication and contributions.

Appendix A. Supplementary data

Supplementary data to this article can be found online at https://doi.org/10.1016/j.ebiom.2019.08.037.

References

[1] Razumilava N, Gores GJ. Cholangiocarcinoma. Lancet. 2014;383(9935):2168–79.
[2] Nakamura H, Arai Y, Totoki Y, Shirota T, Elzawahry A, Kato M, et al. Genomic spectra of biliary tract cancer. Nat Genet 2015;47(9):1003–10.
[3] Rizvi S, Gores GJ. Pathogenesis, diagnosis, and management of cholangiocarcinoma. Gastroenterology. 2013;145(6):1215–29.
[4] Jostins L, Barrett JC. Genetic risk prediction in complex disease. Hum Mol Genet 2011;20(R2):R182–8.
[5] Low SK, Takahashi A, Mushiroda T, Kubo M. Genome-wide association study: a useful tool to identify common genetic variants associated with drug toxicity and efficacy in cancer pharmacogenomics. Clin Cancer Res 2014;20(10):2541–52.
[6] Li XX, Dong Y, Wang W, Wang HL, Chen YY, Shi GY, et al. Emodin as an effective agent in targeting cancer stem-like side population cells of gallbladder carcinoma. Stem Cells Dev 2013;22(4):554–66.
[7] Yuan D, Huang S, Berger E, Liu L, Gross N, Heinzmann F, et al. Kupffer cell-derived Tnf triggers cholangiocellular tumorigenesis through JNK due to chronic mitochondrial dysfunction and ROS. Cancer Cell 2017;31(6) 771–89 e6.
[8] Costa A, Scholer-Dahirel A, Mechta-Grigoriou F. The role of reactive oxygen species and metabolism on cancer cells and their microenvironment. Semin Cancer Biol 2014;25:23–32.
[9] Okon IS, Coughlan KA, Zhang M, Wang Q, Zou MH. Gefitinib-mediated reactive oxygen specie (ROS) instigates mitochondrial dysfunction and drug resistance in lung cancer cells. J Biol Chem 2015;290(14):9101–10.
[10] Geetha A. Evidence for oxidative stress in the gall bladder mucosa of gall stone patients. J Biochem Mol Biol Biophys 2002;6(6):427–32.
[11] Benson AB 3rd, D'Angelica MI, Abrams TA, Are C, Bloomston PM, Chang DT, et al. Hepatobiliary cancers, version 2.2014. J Natl Compr Canc Netw 2014;12(8):1152–82.
[12] Chu X, Pan CM, Zhao SX, Liang J, Gao GQ, Zhang XM, et al. A genome-wide association study identifies two new risk loci for Graves' disease. Nat Genet 2011;43(9):897–901.
[13] Zhan M, Chen G, Pan CM, Gu ZH, Zhao SX, Liu W, et al. Genome-wide association study identifies a novel susceptibility gene for serum TSH levels in Chinese populations. Hum Mol Genet 2014;23(20):5505–17.
[14] Hanley JA, McNeil BJ. The meaning and use of the area under a receiver operating characteristic (ROC) curve. Radiology. 1982;143(1):29–36.
[15] Livak KJ, Schmittgen TD. Analysis of relative gene expression data using real-time quantitative PCR and the 2(−Delta Delta C(T)) method. Methods. 2001;25(4):402–8.
[16] Eruslanov E, Kusmartsev S. Identification of ROS using oxidized DCFDA and flow-cytometry. Methods Mol Biol 2010;594:57–72.
[17] Singh A, Wu H, Zhang P, Happel C, Ma J, Biswal S. Expression of ABCG2 (BCRP) is regulated by Nrf2 in cancer cells that confers side population and chemoresistance phenotype. Mol Cancer Ther 2010;9(8):2365–76.
[18] Tomayko MM, Reynolds CP. Determination of subcutaneous tumor size in athymic (nude) mice. Cancer Chemother Pharmacol 1989;24(3):148–54.
[19] Dixon AL, Liang L, Moffatt MF, Chen W, Heath S, Wong KC, et al. A genome-wide association study of global gene expression. Nat Genet 2007;39(10):1202–7.
[20] Fairfax BP, Makino S, Radhakrishnan J, Plant K, Leslie S, Dilthey A, et al. Genetics of gene expression in primary immune cells identifies cell type-specific master regulators and roles of HLA alleles. Nat Genet 2012;44(5):502–10.
[21] Sur I, Tuupanen S, Whitington T, Aaltonen LA, Taipale J. Lessons from functional analysis of genome-wide association studies. Cancer Res 2013;73(14):4180–4.
[22] Consortium EP, Birney E, Stamatoyannopoulos JA, Dutta A, Guigo R, Gingeras TR, et al. Identification and analysis of functional elements in 1% of the human genome by the ENCODE pilot project. Nature. 2007;447(7146):799–816.
[23] Gaffney DJ. Global properties and functional complexity of human gene regulatory variation. PLoS Genet 2013;9(5):e1003501.
[24] Lecca P. Methods of biological network inference for reverse engineering cancer chemoresistance mechanisms. Drug Discov Today 2014;19(2):151–63.
[25] Kong Y, Peng Y, Liu Y, Xin H, Zhan X, Tan W. Twist1 and snail link hedgehog signaling to tumor-initiating cell-like properties and acquired chemoresistance independently of ABC transporters. Stem Cells 2015;33(4):1063–74.
[26] Kathawala RJ, Gupta P, Ashby CR Jr, Chen ZS. The modulation of ABC transporter-mediated multidrug resistance in cancer: a review of the past decade. Drug Resist Updat 2015;18:1–17.
[27] Tak E, Lee S, Lee J, Rashid MA, Kim YW, Park JH, et al. Human carbonyl reductase 1 upregulated by hypoxia renders resistance to apoptosis in hepatocellular carcinoma cells. J Hepatol 2011;54(2):328–39.
[28] Udler M, Maia AT, Cebrian A, Brown C, Greenberg D, Shah M, et al. Common germline genetic variation in antioxidant defense genes and survival after diagnosis of breast cancer. J Clin Oncol 2007;25(21):3015–23.
[29] Kohler UA, Bohm F, Rolfs F, Egger M, Hornemann T, Pasparakis M, et al. NF-kappaB/RelA and Nrf2 cooperate to maintain hepatocyte integrity and to prevent development of hepatocellular adenoma. J Hepatol 2016;64(1):94–102.
[30] Ni HM, Woolbright BL, Williams J, Copple B, Cui W, Luyendyk JP, et al. Nrf2 promotes the development of fibrosis and tumorigenesis in mice with defective hepatic autophagy. J Hepatol 2014;61(3):617–25.
[31] Shibata T, Kokubu A, Gotoh M, Ojima H, Ohta T, Yamamoto M, et al. Genetic alteration of Keap1 confers constitutive Nrf2 activation and resistance to chemotherapy in gallbladder cancer. Gastroenterology. 2008;135(4):1358–68 (68 e1–4).
[32] Yu KD, Huang AJ, Fan L, Li WF, Shao ZM. Genetic variants in oxidative stress-related genes predict chemoresistance in primary breast cancer: a prospective observational study and validation. Cancer Res 2012;72(2):408–19.
[33] Yamada D, Kobayashi S, Wada H, Kawamoto K, Marubashi S, Eguchi H, et al. Role of crosstalk between interleukin-6 and transforming growth factor-beta 1 in epithelial-mesenchymal transition and chemoresistance in biliary tract cancer. Eur J Cancer 2013;49(7):1725–40.
[34] Razumilava N, Gores GJ. Building a staircase to precision medicine for biliary tract cancer. Nat Genet 2015;47(9):967–8.
[35] Sato-Otsubo A, Sanada M, Ogawa S. Single-nucleotide polymorphism array karyotyping in clinical practice: where, when, and how? Semin Oncol 2012;39(1):13–25.

[36] Matsunaga T, Yamaji Y, Tomokuni T, Morita H, Morikawa Y, Suzuki A, et al. Nitric oxide confers cisplatin resistance in human lung cancer cells through upregulation of aldo-keto reductase 1B10 and proteasome. Free Radic Res 2014;48(11):1371–85.
[37] Pak JH, Son WC, Seo SB, Hong SJ, Sohn WM, Na BK, et al. Peroxiredoxin 6 expression is inversely correlated with nuclear factor-kappaB activation during Clonorchis sinensis infestation. Free Radic Biol Med 2016;99:273–85.
[38] Chang CW, Chen YS, Chou SH, Han CL, Chen YJ, Yang CC, et al. Distinct subpopulations of head and neck cancer cells with different levels of intracellular reactive oxygen species exhibit diverse stemness, proliferation, and chemosensitivity. Cancer Res 2014;74(21):6291–305.
[39] Samatiwat P, Prawan A, Senggunprai L, Kukongviriyapan V. Repression of Nrf2 enhances antitumor effect of 5-fluorouracil and gemcitabine on cholangiocarcinoma cells. Naunyn Schmiedebergs Arch Pharmacol 2015;388(6):601–12.
[40] Guan L, Zhang L, Gong Z, Hou X, Xu Y, Feng X, et al. FoxO3 inactivation promotes human cholangiocarcinoma tumorigenesis and chemoresistance through Keap1-Nrf2 signaling. Hepatology. 2016;63(6):1914–27.
[41] Suphim B, Prawan A, Kukongviriyapan U, Kongpetch S, Buranrat B, Kukongviriyapan V. Redox modulation and human bile duct cancer inhibition by curcumin. Food Chem Toxicol 2010;48(8–9):2265–72.
[42] Wandee J, Prawan A, Senggunprai L, Kongpetch S, Kukongviriyapan V. Metformin sensitizes cholangiocarcinoma cell to cisplatin-induced cytotoxicity through oxidative stress mediated mitochondrial pathway. Life Sci 2019;217:155–63.
[43] Song X, Wang Z, Liang H, Zhang W, Ye Y, Li H, et al. Dioscin induces gallbladder cancer apoptosis by inhibiting ROS-mediated PI3K/AKT signalling. Int J Biol Sci 2017;13(6):782–93.